

1 **Extreme flood events reconstruction spanning the last century in the El Bibane lagoon**
2 **(Southeast of Tunisia): a multi-proxy approach**

3 **Aida Affouri^{a,b}, Laurent Dezileau^b and Nejib Kallel^a**

4 a : Laboratoire Georessources, Matériaux, Environnements et changements globaux,
5 LR13ES23 (GEOGLOB), Faculté des Sciences de Sfax, BP1171, Sfax 3000, Université de
6 Sfax, Tunisie.

7 b : Geosciences Montpellier, CNRS/INSU, UMR 5243, Université Montpellier, Montpellier,
8 France.

9 *Corresponding authors:* aidaemna@yahoo.fr (A. Affouri) and [dezileau@gm.univ-](mailto:dezileau@gm.univ-montp2.fr)
10 [montp2.fr](mailto:dezileau@gm.univ-montp2.fr) (L. Dezileau)

11 **Abstract**

12 Climate models project that rising atmospheric carbon dioxide concentrations will increase
13 the frequency and the severity of some extreme weather events. The flood events represent a
14 major risk for populations and infrastructures settled on coastal lowlands. Recent studies of
15 lagoon sediments have enhanced our knowledge on extreme hydrological events such as
16 paleo-storms and on their relation with climate change over the last millennium. However few
17 studies have been undertaken to reconstruct past flood events from lagoon sediments. Here,
18 the past flood activity was investigated using a multi-proxy approach combining
19 sedimentological and geochemical analysis of surfaces sediments from the Southeast of
20 Tunisia catchment in order to trace the origin of sediment deposits in the El Bibane lagoon.
21 Three sediment sources were identified: marine, fluvial, and aeolian. When applying this
22 multi-proxy approach on the core BL12-10, recovered from the El Bibane lagoon, we can see
23 that finer material, high content of the clay and silt, and high content of the elemental ratios
24 (Fe/Ca and Ti/Ca) characterize the sedimentological signature of the paleoflood levels
25 identified in the lagoonal sequence. For the last century which is the period covered by the

26 BL12-10 short core, three paleo-flood events were identified. The age of these flood events
27 have been determined by ^{210}Pb and ^{137}Cs chronology and give age of AD 1995 ± 6 , AD 1970
28 ± 9 and AD 1945 ± 9 . These results show a good temporal correlation with historical flood
29 events recorded in the Southern of Tunisia in the last century (A.D 1932, A.D 1969, A.D 1979
30 and A.D 1995). Our finding suggests that reconstruction of the history of the hydrological
31 extreme events during the upper Holocene is possible in this location, by the use of the
32 sedimentary archives.

33 **Keywords:** El Bibane Lagoon; watershed basin; surface sediments; geochemistry; grain size;
34 paleo-floods, upper Holocene, Southeast Tunisia.

35 **1. Introduction**

36 The Mediterranean region has experienced numerous extreme coastal events, such as flood
37 events which caused casualties and economic damages (Lionello et al., 2006). However, the
38 meteorological instrumental records are limited to only a few decades, especially in Southern
39 Mediterranean countries. Geological data offer a way to reconstruct the historical records of
40 intense flood events. Deciphering records of extreme precipitation and damaging floods
41 preserved in geologic archives enables society to understand and plan for floods in the future
42 (Parris et al., 2010). The importance of studying trees, river and lake sediments has already
43 been shown for reconstructing extreme flooding events (Baker, 1989; Ely et al., 1993; Brown
44 et al., 2000; Benito et al., 2003; Wolfe et al., 2006; Moreno et al., 2008; Wilhelm et al., 2012;
45 St. George and Nielsen, 2003; Gilli et al., 2013). Few studies have been undertaken to
46 reconstruct past flood events from lagoon sediments (Raji, 2014). Most of the studies were
47 interested to flooding associated with both hurricanes and tsunamis where overwash deposits
48 are preserved within back-barrier lagoons and salt ponds can provide a mean for documenting
49 previous flooding activity (Liu & Fearn, 1993; Donnelly and Woodruff, 2007; Sabatier et al.,
50 2008; Dezileau et al., 2011, 2016; Raji et al., 2015; Degeai et al., 2015). Heavy rain flooding

51 events recorded within these lagoon environments are still poorly documented. Moreover,
52 reconstruction of past flood events from sedimentary archives has been poorly studied in
53 Tunisia. Some fluvial archives have been used to reconstruct past flood events in the northern
54 part of Tunisia (Zielhofer et al. 2004; Zielhofer and Faust; 2008) but not in the southern part.
55 In this study we tried to reveal the importance of lagoonal archives to reconstruct past flood
56 activities under a semi-arid environment in southern part of Tunisia, studying the paleo-floods
57 from high resolution geochemical and sedimentological analyses. The first aim of this study
58 was to identify the different sediment sources and to retrace the marine, the fluvial and the
59 aeolian contributions to the sedimentation in the El Bibane Lagoon. The second aim was to
60 reconstruct flood events from the lagoonal archives during the last century. To reach these
61 objectives, we undertook the calibration of the sedimentological and geochemical proxy data
62 with historical flood records.

63 **2. Study site: El Bibane Lagoon and its watershed**

64 Morphologically, Southern Tunisia known as the Tunisian platform includes two
65 distinguished morpho-tectonic domains (Fig. 1) namely: The Djeffara (Inner domain) and the
66 Dahar (Outer domain). The Djeffara extends over all the coastal plain from Gabes
67 (Southeastern Tunisia) to the Libyan borders. It is limited to the west by the Matmata and the
68 Dahar mountains and to the east by the Gulf of Gabes and the Mediterranean Sea. The Dahar
69 belongs to the Saharan platform domain and is constituted by successions sequences ranging
70 in age from the Late Permian to the Late Cretaceous (Fig. 1). The lithostratigraphic
71 successions could be summarized as follows: The Early–Middle Triassic sequence in the
72 Dahar plateau is mainly constituted by continental sandstone, conglomerate and clay; whereas
73 the Late Triassic outcrops exhibit shallow marine carbonate (Busson, 1967). The Jurassic
74 series are represented by a thick Liassic evaporitic sequence, Dogger marine carbonate and
75 late Jurassic–Neocomian mixed facies with continental predominance (Bouaziz et al., 2002).

76 The Cretaceous series represents a general succession from neritic, lagoonal and continental
77 facies (Mejri et al., 2006). The Late Cretaceous is characterized by thick shallow marine
78 carbonates-marl sequences and covered by sand dunes of the Eastern Saharan Erg.

79 The Mio-Pliocene series represent the substratum of the coastal plain of Djeffara. Jedoui
80 et al. (1998) subdivided these series into two principal facies: (1) the red coloured clays rich
81 in gypsum and (2) the sands which locally associated with conglomerates and grey clays. The
82 Pleistocene marine deposits of the Southeast Tunisian coastal zone assigned to the
83 "Tyrrhenian" (marine isotopic stage 5e) overly unconformably the Mio-Pliocene. These
84 deposits form a ridge parallel to the actual coast. They show the superposition of two units
85 described by Jedoui et al. (2002) as the lower "quartz-rich unit" and the upper "carbonate
86 unit" with *Strombus bubonius*.

87 The study area is focused on the El Bibane Lagoon and its watershed (El Bibane Lagoon:
88 33° 15' 01"N-11° 15' 41"E; Fig. 1). This lagoon which has an elongated elliptic form (33 x10
89 km) and a major WNW-ESE axis covers an area of about 230 Km². It has a maximum water
90 depth of 6m in the middle part of the basin (Guélorget et al., 1982; Medhioub, 1984). The
91 Eastern periphery of the EBL is partially separated from the Mediterranean Sea (Gulf of
92 Gabes) by two peninsulas namely El Gharbi (western) and Ech Chargui (eastern), each of
93 about twelve kilometres long (Medhioub, 1979). These two peninsulas, called slob, are cut at
94 their mid-part by nine small islets and channels: the zone of connection with the
95 Mediterranean waters (Medhioub & Perthuisot, 1981). The two slob are represented by
96 emerged Tyrrhenian aeolian littoral dunes and carbonate sand beach (Jedoui, 2000; Jedoui et
97 al., 2002). The El Bibane Lagoon has a microtidal regime where tidal amplitude varies from
98 0.8 to 1.5 m (Davaud and Septfontaine, 1995; Sammari et al., 2006). The intertidal flats are
99 flooded and exposed daily at regular intervals during the periodically rising and retreating
100 tide. Supratidal flats are flooded at irregular intervals during spring tides or strong onshore

101 winds (Bouougri & Porada, 2012). The El Bibane lagoon is relatively unaffected by human
102 activities (Pilkey, 1989; Ounalli, 2001) where it is only exploited by traditional fisheries
103 (Guélorget et al., 1982).

104 **3. Climate and hydrology**

105 The southeastern Tunisia region is characterized by a pre-Saharan and arid to semi-arid
106 climate. The hot season extends beyond the summer (Amari 1984; Ferchichi, 1996; Hamza,
107 2003) and the number of sunny days may reach 64.4%. The rainfall is low with an annual
108 average that does not exceed 200 mm (Hamza, 2003). Furthermore, rainfall is very
109 fluctuating with high inter-annual variability and intensity. Most of the rainfall is
110 concentrated within 30 days/year (Genin and Sghaier, 2003) leading to high fluctuations in
111 water discharge. The highest precipitation occurs mainly in October to March while in the
112 summer months there are drought conditions.

113 The annual precipitations of Medenine and Tataouine stations during the last century were
114 obtained from the Tunisian General Administration of Water Resources (DGRE, 2010, Fig.2).
115 Five major enhanced precipitation events were recorded from these two stations (i.e. A.D
116 1932, A.D 1969, A.D 1979, A.D 1984 and A.D 1995). These pluvial episodes have induced
117 large flood events in the Fessi River watershed (Poncet, 1970; Bonvallot, 1979; Oueslati,
118 1999; Boujarra and Ktita 2009; Fehri, 2014).

119 **4. Materials and Methods**

120 **4.1. Materials**

121 Eighteen surface sediment samples were collected from the watershed (Jerba, Zarzis,
122 Medenine, Tataouine and Ben Guerdane localities) in order to assess the origin of the material
123 transported into lagoon (Fig. 3). The location of all sampling stations was recorded by GPS
124 (GPSmap 60, Garmin, Table 1). The main potential sediment sources were sampled in order
125 to characterize their sedimentological and chemical signatures as follows:

- 126 - three samples from the beach area (S1, S2 and S3) representing the marine source,
127 - ten samples (S7 to S16) from Fessi River catchment representing the fluvial/river
128 sources,
129 - two dune samples (S17 and S18) representing the eolian component.
130 - three surface samples (S4 to S6) from El Bibane lagoon have been selected to
131 represent the present-day sedimentation. The S6 representing the first three
132 centimeters of a lagoon sediment core BL12-10 was used to characterize the surface
133 sediments samples.

134 Moreover, to reconstruct recent flood events occurred in the studied area, a short
135 sediment core (BL12-10, 40 cm length; Latitude: 33°14'58.7"; Longitude: 11°10'3.7" Fig.3)
136 was recovered from the El Bibane Lagoon (EBL) by a hand corer 75mm diameter PVC tube
137 in the southern part of the lagoon, at 35 km from the Fessi River delta and 14 Km from the
138 connection with the sea.

139 **4.2. Analytical methods**

140 **4.2.1. Sedimentological and geochemical analysis**

141 The BL12-10 core was first split, photographed and logged in detail. Elemental
142 geochemical analyses by energy-dispersive X-ray fluorescence spectrometry were undertaken
143 with a hand-held Niton XL3t. Measurements were realized on the watershed surface samples
144 and each 2 cm along the BL12-10 core. BL12-10 core and surface samples had been covered
145 with a 4µm thin Ultralene film to avoid contamination of the XRF measurement unit and the
146 desiccation of the sediment (Richter et al., 2006). The elemental analyses from XRF
147 measurement were performed in mining type ModCF prolene mode. These data show directly
148 concentrations in ppm or percentage values. This is a semi-quantitative measurement.
149 International powder standards (NIST2702 and NIST2781) were used to assess the analytical
150 error and accuracy of measurement, which are lower than 5% for Ti, Cr, Fe, Zn, Pb, between

151 5 and 15% for Ca, Mn, As, Rb, Sr, and between ca. 15 and 25% for K and Co.

152 Laser grain-size analyses were achieved with a Beckmann-Coulter LS13320 Particle
153 Size Analyser (Geosciences Montpellier). Grain-size analyses were performed on surface
154 samples and on the BL12-10 sequence with an average interval of 1 cm. Each sample was
155 sieved through a 1 mm mesh, suspended in deionised water and gently shaken to achieve
156 disaggregation. Ultrasound was used to avoid particles flocculation of sediment in the fluid
157 module of the granulometer. For each sample, a small homogeneous amount of sediment was
158 mixed in deionized water, then sieved at 1.5 mm diameter before pouring in the Fluid
159 Module of the Particle Sizer until to obtain an optimal obscuration rate between 7 and 12% in
160 the Fraunhofer optical cell. The time of background and sample measurement was set to 90 s
161 and sonication was applied during the measurement of the sample in order to improve the
162 dispersion of fine particles in the fluid. Each sample was measured twice and the good
163 repeatability of measurement was verified according to the statistics from the international
164 standard ISO 13320-1.

165 GRADISTAT program version 4.0 (Blott, 2000) was used for grain size statistical
166 analysis. The following sample statistics are calculated using the Method of Moments in
167 Microsoft Visual Basic programming language: mean, mode(s), sorting (standard deviation),
168 skewness and kurtosis. Grain size parameters are calculated arithmetically, geometrically (in
169 microns) and logarithmically (using the phi scale) (Krumbein and Pettijohn, 1938). Linear
170 interpolation is also used to calculate statistical parameters by the Folk and Ward (1957)
171 graphical method and derive physical descriptions (such as “very coarse sand” and
172 “moderately sorted”).

173 Finally, the percentage of the granulometric classes $<2\mu\text{m}$, 2-63 μm and 63-2000 μm , which
174 stand for clay, silt and sand fractions, respectively, were calculated.

175 **4.2.2. BL12-10 core dating**

176 Dating of sedimentary layers was carried out using ^{210}Pb and ^{137}Cs methods on a
177 centennial timescale. The ^{137}Cs and $^{210}\text{Pb}_{\text{ex}}$ activities analyses were performed on the fraction
178 $< 150\mu\text{m}$ by gamma spectrometry using a CANBERRA Broad Energy Ge (BEGe) detector
179 (CANBERRA BEGe 3825). The sediment was then finely crushed after drying, and
180 transferred into small tubes (diameter 14 mm), and stored for more than 3 weeks to ensure
181 equilibrium between ^{226}Ra and ^{222}Rn . Generally, counting times of 24 to 48 h were required to
182 reach a statistical error of less than 10% for $^{210}\text{Pb}_{\text{ex}}$ in the deepest samples and for the 1963
183 ^{137}Cs peak. Activities of ^{210}Pb were determined by integrating the area of the 46.5-keV photo-
184 peak. ^{226}Ra activities were determined from the average of values derived from the 186.2-keV
185 peak of ^{226}Ra and the peaks of its progeny in secular equilibrium with ^{214}Pb (295 and 352
186 keV) and ^{214}Bi (609 keV). In each sample, the (^{210}Pb unsupported) $_{\text{ex}}$ activities were calculated
187 by subtracting the (^{226}Ra supported) activity from the total (^{210}Pb) activity. We then used the
188 Constant Flux/Constant Sedimentation (CFCS) model and the decrease in $^{210}\text{Pb}_{\text{ex}}$ to calculate
189 the sedimentation rate (Goldberg, 1963). The uncertainty of the sedimentation rate obtained
190 by this method was derived from the standard error of the linear regression of the CFCS
191 model.

192 ^{137}Cs was studied on the core BL12- 10 in order to assess sediment accumulation rates
193 and chronology of the first 30 centimetres of the core. ^{137}Cs ($t_{1/2} = 30.1$ yr) is an
194 anthropogenic radionuclide. It entered the environment in response to atmospheric nuclear
195 tests from 1954 to 1980 AD that induced global fallouts (the first year of atmospheric releases
196 was 1953 AD, whereas the maximum atmospheric production is reached in 1963 AD. ^{137}Cs
197 depth profiles have been extensively used in various environments to assess sediment
198 accumulation rates (Nittrouer et al., 1984; He and Walling, 1996; Radakovitch et al., 1999;
199 Frignani et al., 2004).

200 **4.2.3 Statistical analyses**

201 Statistical methods were applied to complete and refine the analysis. Principal
202 Component Analysis (PCA) is widely used statistical techniques in environmental
203 geochemistry. This multivariate approaches is used to reduce the large number of variable that
204 result from XRF analysis. Principal Component Analysis (PCA) was applied to elements in
205 order to distinguish the different sediment sources of surface sediments and link them to the
206 geochemical processes or proprieties. In the present work, the dataset contains 18 samples,
207 each of which includes concentration of 8 elements (Ca, Sr, Fe, K, Al, Ti, Si and Zr). Data are
208 presented in the form of elemental concentration (8 variables). In this study, a statistical
209 analysis was performed using the STATITCF (1987) which is based on variables and it is
210 suitable for identifying the associations of variables with a set of observations. A
211 representation quality of the parameters (positions in the factorial plane) was then performed.

212 **5. Results**

213 **5.1. Surface sediments**

214 **5.1.1. Sediment description: grain size and morphology**

215 Grain size analysis and binocular observation of the surface sediment samples have
216 permitted to characterize three groups of sediments as follows, depending on the
217 environmental setting: Marine, Fluvial and Aeolian sources (Fig. 4 and 5). The first group
218 encompasses sediment samples (S1, S2 and S3) collected along the coastal zone from Jerba to
219 Zarzis beaches and the lido of El Bibane Lagoon. In this marine area, surface sediments are
220 composed of a mixture of coarse sub-rounded quartz grains, mollusc shells and foraminifera
221 (Fig. 4). The grain size analysis (Table 2) of samples S1 and S2 show unimodal distributions
222 in 169 μ m and 203 μ m, respectively indicating moderately sorted fine sand sediments (Folk,
223 1954; Folk and Ward, 1957; Fig. 5). The sample S3 is muddy sand namely very coarse silty
224 to coarse sand sediment with unimodal distribution in 518 μ m.

225 The second group of samples (S7, S8, S9, S10, S11, S12, S13, S14, S15 and S16) came
226 from the El Bibane delta and the Fessi River. It is assigned as the fluvial source. Binocular
227 observations of the samples reveal reddish-brown heterogeneous particles composed mainly
228 of shiny angular to sub angular quartz grains. Some grains display rust colour with iron oxide
229 (Fig. 4). Figure 5 displays that the fluvial source has a unimodal to multimodal distribution
230 with two or three modes. In order to obtain the best resolution in the identification of the
231 fluvial source, we choose to use the sediment samples which were collected only along the
232 River Fessi: S9, S10, S12 and S13. These surface sediment samples show a decrease in the
233 mean grain size from upstream to downstream of the River Fessi watershed (Fig. 6). The
234 decrease in the mean grain size could be explained by a strong change of the topographic
235 slope around Tataouine (located at approximately 85 km from the lagoon). Here, the coarser
236 material is deposited and the finer material is transported further by the river. These finer
237 sediments are deposited in the low plain of the river and in the El Bibane lagoon. Therefore,
238 we suggest that S9 and S10 (collected between Tataouine and the lagoon) characterize the
239 fluvial component in the lagoon. The grain size distribution for S9 is unimodal with a mean
240 grain size around 96 μm indicating a moderately sorted muddy sand. The corresponding size
241 range very coarse silty/very fine sand. Sample S10 is fine silt with trimodal distribution in
242 7 μm , 26 μm and 73 μm , and poorly sorted mud sediment type. These characteristics will serve
243 to identify the fluvial source into the lagoon.

244 The third group consists of two samples (S17 and S18) recovered in the Aeolian sand
245 dunes of southern Tunisia. They are composed of homogenous dark yellow sand with angular
246 grains; some of them are coated by iron oxide (Fig. 4). Unimodal distribution in 116 μm
247 (Table 2) characterizes the aeolian samples S17 and S18. These samples are well (S18) to
248 very well sorted (S17) and correspond to very fine sand. The characteristics of this group will
249 serve to identify the aeolian sand dune source.

250 The El Bibane Lagoon surface sediments samples S4, S5 and S6 were characterized by
251 multimodal grain size distribution (Table 2, Fig. 5). The grain size distribution of sample S4
252 shows very poorly sorted sandy mud with trimodal distribution at 154 μ m, 96 μ m and 31 μ m,
253 which indicates a very fine sand/very coarse silt. The sample S5 is very coarse silty/very fine
254 sand sediment, with a bimodal distribution in 106 μ m and 429 μ m, poorly sorted muddy sand.
255 The sample S6 is unimodal, with a mode in 116 μ m. It is moderately sorted very coarse
256 silty/fine sand sediment with a muddy sand texture (Folk, 1954; Folk and Ward, 1957).

257 **5.1.2. Distribution of major and trace elements**

258 The spatial distribution of major and trace elements in surface sediments collected in the
259 El Bibane lagoon and in all the area mainly along the Fessi River are displayed in figure 7.

260 The iron (Fe) shows its highest percentages in the Fessi River samples (0.53-1.52%).
261 Lower values characterise the aeolian dunes (0.38-0.4%) whereas this element is totally
262 absent in marine sediments (Table 3). The same distribution pattern is also observed for Ti, K
263 and Al. The highest contents of these elements in the Fessi River samples contrast with the
264 lowest ones retrieved in the marine surface sediment. Aeolian dunes are characterised by
265 intermediate values. These four elements will thus be used as indicators of terrigenous input
266 of material to the lagoon.

267 Calcium (Ca) and Strontium (Sr) in the sediment are usually associated to the carbonate
268 fraction, which can be either of allochthonous or autochthonous origin. In the sediments,
269 carbonates are mainly of biogenic origin. In fact, due to its compatible ionic radius, Sr can
270 replace Ca in calcite, but remains however as trace element (Fig.7). Nevertheless, both
271 elements show the same distribution pattern. Marine surface sediments are associated with the
272 highest values (Ca \approx 14, 7%; Sr \approx 1548 ppm) whereas the lowest values and thus the lowest
273 calcite contents are retrieved in dune samples (Ca \approx 0.8%; Sr \approx 52 ppm). Intermediate

274 concentrations are associated with the Fessi River catchment ($\text{Ca} \approx 7\%$; $\text{Sr} \approx 150$ ppm) (Table
275 3).

276 Silicon (Si) and Zircon (Zr) follow similar spatial distribution pattern (Fig. 7). Higher
277 content of these elements are observed in the River catchment samples ($\text{Si} \approx 20\%$; $\text{Zr} \approx 300$
278 ppm) and in the aeolian dune samples ($\text{Si} \approx 33\%$; $\text{Zr} \approx 400$ ppm), whereas marine sediments
279 show generally lower contents ($\text{Si} \approx 10\%$; $\text{Zr} \approx 41$ ppm) (Table 3).

280 **5.1.3. Principal component analysis (PCA)**

281 We used Principal Component Analysis (PCA) to identify the main factors controlling
282 the chemical composition of the catchment and El Bibane lagoon surface sediments and to
283 identify different groups of common origin and process. Application of Principal Component
284 Analysis (PCA) varimax rotation has permitted to identify two components that explained
285 83% of the total variance (Fig. 8). Factor 1 account for 64.46% of total variance. It is
286 characterized by high positive loadings for Fe, Ti, K, and Al which indicates the dominance
287 of alumino-silicates minerals in surface sediments (Spagnoli et al., 2008; Plewa et al., 2012).
288 These elements are prevailing in the river surface samples and their granulometric
289 distributions display that their grain sizes are in the range of clay and silt. Zr and Si display a
290 moderate positive loading in factor 1 and are high in the Aeolian surface sediments. Zr and Si
291 are associated to silicates originating either from adjacent desert areas by erosion or from
292 western Saharan dunes by storms.

293 Factor 2 account for 17.73% of the total variance (Fig. 8). It shows positive loading for
294 Ca, Sr, Fe and K, whereas Ti, Al, Zr and Si have negative loadings. Ca is high in the marine
295 samples. The high percentage of Ca in these samples is related to both the significant presence
296 of biogenic material and also probably the precipitation of authigenic carbonate. These results
297 corroborate the marine origin of these sediments as revealed by the binocular observations
298 mainly due to the existence of shell debris and confirmed by the grain size distributions.

299 Therefore, we suggested that the first component agreed with the fine fraction of the
300 sediment, which is mainly composed of various types of clay minerals, usually abundant in
301 surface sediments (De Lazzari et al., 2004). On the other hand, factor 2 (Fig. 8) provides a
302 better definition of the relatively carbonate fraction of the sediments. Consequently, these two
303 factors differentiated carbonates from both sand and clay sediments. This method allowed us
304 to label elements of terrigenous source (Fe, Ti, K and Al) from those from in situ marine
305 origin (Ca and Sr). These proxies will be used to reconstruct past flood and storm events with
306 the help of sedimentary archives.

307 **5.1.4. El Bibane lagoon: Main sediment sources**

308 Geochemical parameters as well as grain size data are useful indicators for the
309 detection of significant facies changes in the stratigraphical record (Vött et al., 2002, Zhu &
310 Weindorf, 2009). Statistical analyses of geochemical data have permitted to characterise the
311 different sediment sources around El Bibane lagoon. Ca, Ti and Fe elements have been
312 chosen in order to recognize the contribution of these sources to the surface sediments of the
313 Lagoon. Ca displays its highest abundances in marine area and is lower in sand dunes and
314 river samples. By contrast, Ti characterises the continental source (see section 5.1.2) and
315 shows low contents in marine samples. On the other hand, Fe is present as a maximum in the
316 river samples and as a trace element in marine samples. Taking into account this geographic
317 distribution, Fe/Ca as well as Ti/Ca ratios values would be higher in the continental supply
318 (fluvial and aeolian samples) and lower in the marine source. High Fe/Ca values due to high
319 iron content may also reflect dominating subaerial weathering and oxidation. The Fe/Ca and
320 Ti/Ca ratio values and the position on a Fe/Ca vs. Ti/Ca diagram (Fig. 9) of El Bibane Lagoon
321 surface sediments (samples S4, S5 and S6) are intermediate between the marine and fluvial
322 source. Accordingly, higher Fe/Ca and Ti/Ca ratio in the lagoon sediments would be a signal
323 of more sediment contribution from fluvial source to the lagoon during flooding. As shown

324 before, the Fessi River sediments were characterized by fine material with a grain size which
325 does not exceed 63 μm (case of S9 and S10) (See Chap.5.1.1, page 10).

326 **5.2 Core BL12-10**

327 **5.2.1. ^{210}Pb and ^{137}Cs dating**

328 The measured ^{210}Pb values in the uppermost 30 cm of the BL12-10 core range from
329 14.5 to 0.1 mBq /g (Table 4). In general, the down core distribution of $^{210}\text{Pb}_{\text{ex}}$ values follows a
330 relatively exponential decrease with depth and the “Constant flux: Constant Supply” (CF/CS)
331 sedimentation model was applied. The calculated sedimentation rate (SR) is about 0.48 cm/
332 year. The down core ^{137}Cs activity profile (Fig. 10) shows a maximum at 18 cm depth (Table
333 4). We attributed this maximum to the period of maximum radionuclide fallout in the
334 Northern Hemisphere associated with the peak of atomic weapons testing in 1963. The ^{137}Cs -
335 derived SR (0.37 cm/ year) is lower than that of the ^{210}Pb (Fig. 10). The difference between
336 the two methods could be explained by a change of the accumulation rate between the
337 beginning and the last part of the 20th century.

338 **5.2.2 Sedimentary and geochemistry**

339 The sediment sequence from El Bibane lagoon presented in this study come from the
340 core BL12-10 recovered in the nearest part of the delta of Fessi River in May 2012. This
341 study proposes the preliminary analyses performed on the first 30 cm only although the whole
342 BL12-10 core length is 90 cm. The BL12-10 core is composed of coarse-grained layers of
343 siliciclastic sand and shell fragments inter-bedded with organic rich dark grey fine grained
344 sediment (mud) of clay and silt (Fig. 11). These coarse layers are interbedded with three mud
345 layers from 6 to 10 cm, 14 to 18 cm and 26 to 30 cm core depth (Fig. 11). The thickest fine
346 grained layers are typically composed of clay and silt sediments. The core BL12-10 is
347 dominated by the bimodal and trimodal grain size distributions. These distributions were
348 labeled as very coarse silty to very fine sand, poorly to very poorly sorted, fine skewed with

349 leptokurtic distribution (Table 5). Down-core profiles of heavy and light elements through the
350 depth also delineate the different units distinguished by sedimentological analysis (Fig.11).
351 Based on their profiles, the first group composed by Fe, Ti, K and Al exhibit similar
352 variations, concentration values are mainly high in fine-grained intervals and are low in
353 coarse-grained intervals. These high values are probably due to high inputs from the Fessi
354 River. The Si and Zr which characterized the second group display a different behaviour than
355 the first group (Fig.11). These two elements are high in the fine sandy intervals. This probably
356 suggests that their highest values are related to aeolian inputs in the lagoon. The Ca and Sr
357 characterised the third group show a reverse distribution pattern by comparison to the first
358 group with higher values in the coarse grained intervals and lower values in the fine grained
359 intervals (Fig.11). Single element concentrations may be sensitive to dilution effects to allow
360 reliable reconstructions of terrestrial climate, elemental ratios often better reflect the origin of
361 the sedimentary material. The measured elemental ratios Fe/Ca and Ti/Ca will be used to
362 reconstruct pas flood events (Fig. 9). A higher Fe/Ca and Ti/Ca ratio in the lagoon sediments
363 would be a signal of more sediment contribution from the Fessi River during flooding.

364 **6. Discussion**

365 **6.1 Paleoflood reconstructions**

366 In order to identify the paleo-flood events of the El Bibane Lagoon, we applied these
367 previously discussed proxies to BL12-10 core samples. The BL12-10 core shows 3 mud
368 layers (clay and silt mixture) preserved in the core which seems to be flood layers, i.e.,
369 coming from fluvial incursions during intense flood events. Multiproxy analysis on these mud
370 layers show that they are characterized by high content in clay+silt, as well as high Fe/Ca and
371 Ti/Ca elemental ratios which represent the sedimentological signature of the River Fessi. The
372 combination of geochemical and grain size data suggest that the BL12-10 core deposits had

373 registered three flood events namely FL1, FL2 and FL3 (Fig. 12). These flood deposits have a
374 thickness of 5cm, 4cm and 2.5cm respectively.

375 Our paleoflood reconstruction has been compared with historical rainfall data of
376 Tataouine and Medenine (DGRE, 2000; Fehri, 2014). A good correlation is observed between
377 instrumental rainfall records and past flood events recorded in the El Bibane lagoon. Based on
378 our age model, FL1 would have occurred around AD 1995 \pm 6 yrs (Fig. 12). This sediment
379 deposit could correspond to the 1995 flood event recorded in hydrological data (Fehri, 2014)
380 and which affected the entire Tataouine region. This flood reached a maximum discharge of
381 1200 m³/s due to a heavy precipitation event during 24 hours (Boujarra and ktita, 2009).
382 These events provoked heavy losses in human lives and agricultural goods (Boujarra and
383 Ktita, 2009). Using the same approach, FL2 would have occurred around AD 1970 \pm 9 yrs, i.e.
384 between AD 1965 to 1980 (Fig.12). Between these dates, two historical extreme flood events
385 are known (AD.1969 and AD.1979) and one flood event of lower magnitude (AD.1972). The
386 1969 flood event is characterized by a heavy precipitation (400 to 600 mm) during 24 to 48
387 (Pias et Stuckmann, 1970, Kallel et al., 1972 and Boujarra and Ktita, 2009). The 1979 flood
388 event is characterized by a heavy precipitation during 4 days (Bonvallot, 1979). Only one
389 horizon corresponds to these events in the BL12-10 core. Consequently, we assume that this
390 unique flood deposit registers a period during which these three high precipitation events
391 occurred (i.e. AD.1969, AD.1972 and AD.1979). The activity of ²¹⁰Pb in this flood deposit is
392 not disturbed; it is homogeneous (Fig. 10). For this reason we assume that no significant
393 erosion happened in the lagoon during this period. During these heavy precipitation events,
394 most of the sedimentary material was deposited in the floodplain, in the lagoon and probably
395 transported to the Mediterranean Sea through the passes. The sedimentation rate
396 corresponding to these events is not very high. The thickness of the sediment layer associated
397 with these flood events is low, i.e. about 5 cm. The grain size and geochemical values of this

398 flood deposit are rather homogeneous. This homogeneity is probably linked to the action of
399 weak bottom currents within the El Bibane lagoon. Finally, since these three extreme flood
400 events are very close together in time (1969-1979) and the sedimentation rate is low, they are
401 recorded as only one sedimentary deposit (FL2) in our archive. The third flood event FL3 was
402 dated at A.D 1945±9 (Fig. 12). It could be associated to the 1932 flood event (Fehri, 2014).
403 This event was characterized by a flash flood event with a precipitation of 449 mm in few
404 days. Bonvallot (1979) demonstrated that this event presents a similar characteristic than that
405 of 1979.

406 El Bibane flood record shows temporal correspondence of flood layers to historical heavy
407 precipitation events. Considering the historical data, we can assume that FL3 flood deposit
408 corresponds to A.D 1932 flood. FL2 flood deposit is associated to A.D 1969, A.D 1972 and
409 A.D 1969 flood events. FL1 flood deposit could be associated to the A.D 1995 flood event
410 (Fig. 12). In this lagoonal environment, one flood deposit is not always associated to a single
411 event but sometimes to two or three events especially when heavy precipitation events are
412 close together in time (i.e. FL2 flood deposit). Moreover these data demonstrate that finer
413 material with a high content of mud (clay+silt), and high ratios of Fe/Ca and Ti/Ca are
414 associated to flood events in the lagoonal sequence. The association of these proxies in the
415 sedimentary sequence of the El Bibane lagoon can therefore be used to reconstruct flood
416 activities in Southeastern Tunisia.

417 **6.2. The El Bibane lagoon: A key region for paleohydrological reconstructions**

418 Lagoon records shows that such costal environments are good study areas to record
419 past climatic and environmental changes, and extreme sea events. These fields of research
420 were successfully applied in the western North Atlantic (Donnelly and Woodruff, 2007),
421 Northwest Florida (Liu and Fearn, 2000; Lane et al., 2011; Das et al., 2013), the Northeastern
422 United States (Parris et al., 2010), the Central Pacific (Toomey et al., 2013), Southern Japan

423 (Woodruff et al., 2009), Western Australia (Nott, 2011), Northeastern New Zealand (Page et
424 al., 2010), Northern Europe (Sorrel et al., 2012), or the Western Mediterranean (Dezileau et
425 al., 2011, 2016; Sabatier et al., 2012; Raji et al., 2015; Degeai et al., 2015). Such studies are
426 still scarce in southern Tunisia, despite the importance of these topics in Mediterranean
427 coastal areas. The El Bibane lagoon is different from the other studied lagoons because it
428 cannot record coastal overwash events. Such particularity is linked to the morphology of
429 barriers that separate this lagoon from the open sea. These barriers consist of two narrow
430 fossil carbonate consolidated peninsula formed during the last interglacial period and reaching
431 10 m elevation (Medhioub, 1979; Jedoui, 2000). Thus they cannot not be over-washed during
432 extreme sea events. However, we have demonstrated from this study that this lagoon could
433 record past flood events during exceptional heavy precipitation episodes that punctuated the
434 recent meteorological and climatic history of Tunisia and North Africa. Trambly et al.,
435 (2013) have analysed the influence of large-scale atmospheric circulation, including the North
436 Atlantic Oscillation (NAO), Mediterranean Oscillation (MO), El Nino-Southern Oscillation
437 (ENSO) and Western Mediterranean Oscillation (WEMO) on precipitations and extreme
438 events in 22 stations located in Algeria, Morocco and Tunisia for the last 50 years. Although
439 some spatial patterns for the different precipitation indices have been identified over Maghreb
440 countries the southern part of Tunisia was only represented by one meteorological station
441 (Gabes). This clearly avoid to identify an homogeneous climatic region, there is a need to
442 include more stations with longer record length. El Bibane lagoon paleoflood record can be
443 of great importance to better understand the physical mechanism responsible for the changes
444 in the frequency and/or the intensity of extreme events in the southern part of Tunisia. It will
445 be interesting to study the natural variability of past flood events in this semi-arid
446 environment through contrasting climatic periods (cold and warm periods). Further coming
447 investigations on long core sediments could clarify the relationship between large-scale

448 atmospheric circulation reconstructions and the major flood periods (Affouri et al., data in
449 progress). Additionally, such studies could be a crucial tool to evaluate the role of
450 Mediterranean paleo-climate on the development and growth of human society.

451 **Conclusion**

452 This study focuses on the sedimentological and geochemical characterization of the main
453 surface sediments sources of El Bibane Lagoon (southeast Tunisia) and its watershed in order
454 to identify the specific signature of paleoflood events recorded in the sedimentary core
455 archives. We used Principal Component Analysis (PCA) to identify the main factors
456 controlling the chemical composition of the catchment and El Bibane lagoon surface
457 sediments and to discriminate between the sources of detrital inputs into the lagoon. Three
458 sediments sources were identified: Marine, fluvial and Aeolian. Our results display that El
459 Bibane Lagoon surface sediment characteristics are situated between marine and river
460 sources. The application of this multi-proxy analysis on the BL12-10 core shows that finer
461 material, high content of mud (clay+silt), as well as high elemental ratios (Fe/Ca and Ti/Ca)
462 typify the sedimentological signature of flood events in the lagoonal sequence. The BL12-10
463 age model based on ^{210}Pb and ^{137}Cs activity profiles have allowed us to identify three periods
464 of past flood events dated at AD 1995±6, AD 1970±9, and 1945±9. The good agreement
465 between our estimated ages and the historical flood events suggests that sedimentological and
466 geochemical data of lagoon sediment cores could be used to reconstruct paleoflood history in
467 South-eastern Tunisia in arid and semi-arid environment during the upper Holocene.

468 **Acknowledgments**

469 Our thanks go to Dr. M. Ouaja, Ph. Blanchemache and J.P. Degai for their help on the field.
470 We also thank Pr. Y. Jedoui and G. Siani for their fruitful suggestions in the discussions. This
471 study is funded by FP7-IRSES MEDYNA 2014-2017, the MISTRALS PALEOMEX and the
472 PHC-UTIQUE N° 14G1002 projects. We are particularly grateful for editor comments of Dr

473 Nathalie Combourieu-Nebout. We thank Maria-Angella Bassetti, MCF-HDR Assistant
474 Professor at the University of Perpignan, France and anonymous reviewers for their helpful
475 comments and their criticism, which led to a considerable improvement of the manuscript.

476 **References**

477 Affouri, A., Dezileau, L., and Kallel, N.: Late Holocene paleoclimatic reconstruction inferred
478 from EL Bibane lagoon (Southeast of Tunisia), in prep.

479 Amari, A. : Contribution à la connaissance hydrologique et sédimentologique de la plateforme
480 des îles Kerkennah Thèse de 3ème cycle. Faculté des Sciences de Tunis, Tunis, 1984.

481 Baker, V.R.: Magnitude and frequency of paleofloods. In: Beven, K., Carling, P. (Eds.),
482 Floods: Hydrological, Sedimentological, and Geomorphological Implications. Wiley,
483 Chichester, pp, 171-183, 1989.

484 Benito, G., Díez-Herrero, A., and Fernández de Villalta, M.: Magnitude and Frequency of
485 Flooding in the Tagus Basin (Central Spain) over the Last Millenium', *Clim. Change*,
486 58, 171–192, 2003.

487 Blott, S.J.: Gradistat version 4.0 - A Grain Size Distribution and Statistics Package for the
488 Analysis of unconsolidated sediments by Sieving or Laser Granulometer. Surface
489 Processes and Modern Environments Research Group, Department of Geology, Royal
490 Holloway, University of London, Egham, Surrey TW20 0EX, 2000.

491 Bonvallet, J.: Comportement des ouvrages de petite hydraulique dans la région de Médenine
492 (Tunisie du Sud) au cours des pluies exceptionnelles de mars 1979, *les Cahiers de*
493 *l'O.R.S.T.O.M, Série Sciences Humaines XVI, 3, 233-249, 1979.*

494 Bouaziz, S., Barrier, E., Souissi, M., Turki, M.M., and Zouari, H.: Tectonic evolution of the
495 northern African margin in Tunisia from paleostress data and sedimentary record,
496 *Tectonophysics 357, 227-253, 2002.*

497 Boujarra, A., and Ktita, A.: Les facteurs de l'amplification de l'inondation de la ville de

498 Tataouine le 24 septembre 1995 (SUD EST TUNISIEN), Risques naturelles en
499 Méditerranée occidentale, p 195-206, 2009.

500 Bouougri, E.H. and Porada, H.: Wind-induced mat deformation structures in recent tidal flats
501 and sabkhas of SE-Tunisia and their significance for environmental interpretation of
502 fossil structures, *Sedimentary Geology*, 263–264, 56–66, 2012.

503 Busson, G. : Le mésozoïque saharien 1^{ère} partie : l'Extrême Sud tunisien. Centre National de la
504 Recherche Scientifique, Paris, Géologie, 8, 204 p, 1967.

505 Brown, S.L., Bierman, P.R., Lini, A., and Southon, J.: 10 000 yr records of extreme
506 hydrologic events. *Geology*, 28, 335-338, 2000.

507 Das, O., Wang, Y., Donoghue, J., Xu, X., Coor, J., Elsner, J., and Xu, Y.: Reconstruction of
508 paleostorm and paleoenvironment history using geochemical proxies archived in the
509 sediments of two coastal lakes in NW Florida. *Quaternary Sci. Rev.*, 68, 142–153, 2013.

510 Davaud, E. and Septfontaine, M.: Post-mortem onshore transportation of epiphytic
511 foraminifera: recent example from the Tunisian coastline, *Journal of Sedimentary
512 Research* 65, 136-142, 1995.

513 Degeai, J.P., Devillers, B., Dézileau, L., Oueslati, H., and Bony, G.: Major storm periods and
514 climate forcing in the Western Mediterranean during the Late Holocene, *Quaternary
515 Science Reviews*, 129, 37-56, 2015.

516 Dezileau, L., Sabatier, P., Blanchemanche, P., Joly, B., Swingedouw, D., Cassou, C.,
517 Castaings, J., Martinez, P., and Von Grafenstein, U.: Intense storm activity during the
518 Little Ice Age on the French Mediterranean coast, *Palaeogeogr. Palaeoclimatol., 299, 289-297,*
519 2011.

520 Dezileau, L., Perez-Ruzafa, A., Blanchemanche, P., Martinez, P., Marcos, C., Raji, O., Van
521 Grafenstein, U.: Extreme storms during the last 6,500 years from lagoonal sedimentary
522 archives in Mar Menor (SE Spain), *Climate of the Past*, 12, 1389-1400, 2016.

523 De Lazzari, A., Rampazzo, G., and Pavoni, B.: Geochemistry of sediments in the Northern
524 and Central Adriatic Sea, *Estuarine, Coastal and Shelf Sciences* 59, 429-440, 2004.

525 Direction Générale des Ressources en Eau (DGRE): *Annuaire hydrométéorologiques 1976*
526 2010, Ministère de l'Agriculture, l'Environnement et les ressources en eau, Tunisie,
527 2010.

528 Donnelly, J. P. and Woodruff, J. D.: Intense hurricane activity over the past 5,000 years
529 controlled by El Nino and the West African monsoon, *Nature*, 447, 465–468, 2007.

530 Ely, L.L., Enzel, Y., Baker, V.R., and Cayan, D.R.: A 5000-year record of extreme flood and
531 climatechange in the southwestern United States. *Science*, 262,410–412, 1993.

532 Fehri, N. : L'aggravation des risques d'inondation en Tunisie : éléments de réflexion. *Physio-*
533 *Géo. Géographie, physique et environnement*, Volume 8, 149-175, 2014.

534 Ferchichi, A., 1996. : Etude climatique en Tunisie présaharienne : proposition d'un nouvel
535 indice de subdivision climatique des étages méditerranéens aride et saharien. *Medit*
536 *(italy)*, 3/96: 46-53.

537 Folk, R.L.: The distinction between grain size and mineral composition in sedimentary rock
538 nomenclature. *Jour. Geology* 62, 344-359,1954.

539 Folk, R. L., and Ward, W. C.: Brazos river bar: A study in the significance of grain size
540 parameters, *Journal of Sedimentary Petrology* 27, 3-26, 1957.

541 Frignani, M., Sorgente, D., Langone, L., Albertazzi, S., and Ravaioli, M. : Behaviour of
542 Chernobyl radiocesium in sediments of the Adriatic Sea off the Po River delta and the
543 Emilia-Romagna coast. *J. Environ. Radioactivity* 71, 299-312, 2004.

544 Genin, D. and Sghaier, M.: *Pratiques et usages des ressources, techniques de lutte et devenir*
545 *des populations rurales, Rapport scientifique final de synthèse, IRA, IRD (Projet Jeffara),*
546 20, 2003.

547 Gilli, A., Anselmetti, F.S., Glur, L., and Wirth, S.B.: Lake Sediments as Archives of
548 Recurrence Rates and Intensities of Past Flood Events, Dating Torrential Processes on
549 Fans and Cones, *Advances in Global Change Research* 47, DOI 10.1007/978-94-007-
550 4336-6 15, 2013.

551 Goldberg, E.: Geochronology with lead-210, International Atomic Energy Agency, 121–131,
552 1963.

553 Guélorget, O., Frisoni, G.F., and Perthuisot, J.P.: Contribution à l'étude biologique de la
554 Bahiret el Biban : lagune du Sud-Est Tunisien, *Mémoires de la Société Géologique de*
555 *France* 144, 173-186, 1982.

556 Hamza, A. : Le statut du phytoplancton dans le golfe de Gabès. Thèse de Doctorat, Université
557 de Sfax, 298, 2003.

558 He and Walling.: Use of fallout Pb-210 measurements to investigate longer-term rates and
559 patterns of overbank sediment deposition on the floodplains of lowland rivers *Earth Surf.*
560 *Proc. Land.*, 21 pp. 141–154, 1996.

561 Jedoui, Y. : Sédimentologie et géochronologie des dépôts littoraux quaternaires:
562 reconstitution des variations des paléoclimats et du niveau marin dans le Sud-Est tunisien.
563 Thèse d'Etat es. Sciences., Fac. Sc. Tunis, Université de Tunis El Manar, 338, 2000.

564 Jedoui, Y., Kallel, N., Fontugne, M., Ben Ismail, M.H., M'Rabet, A., and Montacer, M.: A
565 relative sea-level stand in the middle Holocene of southeastern Tunisia: *Marine Geology.*,
566 147, 123–130, 1998.

567 Jedoui, Y., Davaud, E., Ben Ismaïl, H., and Reyss, J.L.: Analyse sédimentologique des dépôts
568 marins pléistocènes du Sud-Est tunisien: mise en évidence de deux périodes de haut
569 niveau marin pendant le sous-stade isotopique marin 5e (Eémien, Tyrrhénien), *Bulletin*
570 *de la Société Géologique de France* 173, 63-72, 2002.

571 Kallel, R., Colombani, J., Eoche duval, J.M. : Les précipitations et les crues exceptionnelles

572 de l'automne 1969 en Tunisie, publication de la division des ressources en eau,
573 Ressources en eau de Tunisie, 1972.

574 Krumbein, W.C. and Pettijohn, F.J.: Manual of Sedimentary Petrography. Appleton-Century-
575 Crofts, New York, 1938.

576 Lane, P., Donnelly, J.P., Woodruff, J.D., and Hawkes, A.D.: A decadal-resolved
577 paleohurricane record archived in the late Holocene sediments of a Florida sinkhole.
578 Marine Geology 287, 14-30, 2011.

579 Lionello, P., Bhend, J., Buzzi, A., Della-Marta, P., Krichak, S., Jansa, A., Maheras, P., Sanna,
580 A., Trigo, I., and Trigo, R.: Cyclones in the Mediterranean region: climatology and
581 effects on the environment, Developments in Earth and Environmental Sciences, 4, 325-
582 372, 2006.

583 Liu, K.-B., and Fearn, M.L.: Reconstruction of Prehistoric Landfall Frequencies of
584 Catastrophic Hurricanes in Northwestern Florida from Lake Sediment Records.
585 Quaternary Research 54, 238-245. 2000.

586 Liu, K.B. and Fearn, M. L.: Lake-sediment record of late Holocene hurricane activities from
587 coastal Alabama, Geology, 21, 793– 796, 1993.

588 Medhioub, K. : La Bahiret El Bibane. Etude géochimique et sédimentologique d'une lagune
589 du Sud-Est tunisien, Travail du laboratoire de Géologie, Presse de l'école Normale
590 Supérieure, Paris, 13, 150, 1979.

591 Medhioub, K. : Etude géochimique et sédimentologique du complexe paralique de la
592 dépression de ben Guirden: Bahira el Biban, Sabkha bou J'Mel et Sabkha el Medina.
593 Thèse Doctorat es- Sciences, Ecole Normale Supérieur, Paris, 400, 1984.

594 Medhioub, K.and Perthuisot, J.P.: The influence of peripheral sabkhas on the geochemistry
595 and sedimentology of a Tunisian lagoon: Bahiret el Biban, Sedimentology, 28, 679–688.
596 1981.

597 Mejeri, F., Burollet, P.F., and Ben Ferjani, A.: Petroleum geology of Tunisia: A renewed
598 synthesis, Memoir ETAP 22, 233, 2006.

599 Moreno, A., Valero-Garcés, B., Gonzales-Sampériz, P., and Rico, M.: Flood response to
600 rainfall variability during the last 2000 years inferred from the Taravilla Lake record
601 (Central Iberian Range, Spain). *Journal of Paleolimnology* 40, 943–961, 2008.

602 Nittrouer, C.A., DeMaster, D.J., Kuehl, S.A., McKee, B.A., Thorbjarnarson, K.W.: Some
603 questions and answers about the accumulation of fine-grained sediments in continental
604 margin environments. *Geo-Marine Letters*, 4, 211-213. 1984- 1985.

605 Nott, J.: A 6000 year tropical cyclone record from Western Australia. *Quaternary Science*
606 *Reviews* 30, 713-722, 2011.

607 Ounalli, A. : Projet de dessalement d'eau de mer à El Bibane. *Desalination*, 137, 293-296,
608 2001.

609 Oueslati, A.: Les inondations en Tunisie. Publication à compte d'auteur, p. 206, 1999.

610 Page, M.J., Trustrum, N.A., Orpin, A.R., Carter, L., Gomez, B., Cochran, U.A., Mildenhall,
611 D.C., Rogers, K.M., Brackley, H.L., Palmer, A.S., and Northcote, L.: Storm frequency
612 and magnitude in response to Holocene climate variability, Lake Tutira, North-Eastern
613 New Zealand. *Marine Geology* 270, 30-44, 2010.

614 Parris, A.S., Bierman, P.R., Noren, A.J., Prins, M.A., and Lini, A.: Holocene paleostorms
615 identified by particle size signatures in lake sediments from the northeastern United
616 States. *Journal of Paleolimnology* 43, 29-49, 2010.

617 Poncet, J.: La catastrophe climatique de l'automne 1969 en Tunisie, *Annales de Géographie*,
618 vol 79, n°435, p.581-595,1970.

619 Pias, J.and Stuckmann, G.: Les inondations de septembre- octobre 1969 en Tunisie, Partie 2
620 Etude morphologique, UNESCO, Paris, 1970.

621 Pilkey, O.H.: A thumbnail method for beach communities: estimation of long-term beach

622 replenishment requirements, *Shore and Beach*, July, 1988. 23 - 31. 1989.

623 Plewa, K., Meggers, H., Kuhlmann, H., Freudenthal, T., Zabel, M., and Kasten, S.:
624 Geochemical distribution patterns as indicators for productivity and terrigenous input off
625 NW Africa. *Deep Sea Research*, I 66, 51-66, 2012.

626 Raji, O., Dezileau, L., Von Grafenstein, U., Niazi, S., Snoussi, M., and Martinez, P.: Sea
627 extreme events during the last millennium in north-east of Morocco, *Natural Hazards*
628 *Earth, Systems Science Discussion*, 2, 2079-2102, 2015.

629 Raji, O.: Événements extrêmes du passé et paleo-environnements: reconstruction à partir des
630 archives sédimentaires de la lagune Nador, Maroc, Thèse de Doctorat, Université
631 Mohammed V de Rabat. 2014.

632 Radakovitch, O., Charmasson, S., Arnaud, M., Bouisset, and P.: 210Pb and caesium
633 accumulation in the Rhône delta sediments. *Estuar. Coast. Shelf Sci* 48, 77–92. 1999.

634 Richter, T.O., Van der Gaast, S., Koster, B., Vaars, A., Gieles, R., de Stigter, H.C., De Haas,
635 H., and Van Weering, T.C.E.: The Avaatech XRF Core Scanner: technical description
636 and applications to NE Atlantic sediments, In: Rothwell, R.G. (Eds.), *Techniques in*
637 *Sediment Core Analysis: Geological Society of London, Special Publications*, 39–50.
638 2006.

639 Sabatier, P., Dezileau, L., Condomines, M., Briquieu, L., Colin, C., Bouchette, F., Le Duff,
640 M., and Blanchemanche, P.: Reconstruction of paleostorm events in a coastal lagoon
641 (Herault, South of France), *Marine Geol.*, 251, 224–232, 2008.

642 Sabatier, P., Dezileau, L., Colin, C., Briquieu, L., Bouchette, F., Martinez, P., and Von
643 Grafenstein, U.: 7000 years of paleostorm activity in the NW Mediterranean Sea in
644 response to Holocene climate events, *Quaternary Res.*, 77, 1–11, 2012.

645 Sammari, C., Koutitonsky, V.G., Moussa, M.: Sea level variability and tidal resonance in the
646 Gulf of Gabes, Tunisia, *Continental Shelf Research*, 26, 338-350, 2006.

647 Spagnoli, F., Bartholinia, G., Dinelli, E., and Giordano, P.: Geochemistry and particle size of
648 surface sediments of Gulf of Manfredonia (Southern Adriatic Sea), Estuarine, Coastal and
649 Shelf Science 80, 21–30,2008.

650 St. George, S and E. Nielson.: Paleoflood records for the Red River, Manitoba, Canada,
651 derived from anatomical tree-ring signatures: The Holocene 13 (4), 547-555, 2003.

652 STATIT-CF: Services des études statistiques de l'I.T.C.F.

653 Sorrel, P., Debret, M., Billeaud, I., Jaccard, S.L., McManus, J.F., and Tessier, B.: Persistent
654 non-solar forcing of Holocene storm dynamics in coastal sedimentary archives. Nature
655 Geoscience 5, 892-896, 2012.

656 Trambly, Y., El Adlouni, S., and Servat, E.: Trends and variability in extreme precipitation
657 indices over Maghreb countries, Nat. Hazards Earth Syst. Sci., 13, 3235–3248, 2013
658 doi:10.5194/nhess-13-3235-2013.

659 Toomey, M.R., Donnelly, J.P., and Woodruff, J.D.: Reconstructing mid-late Holocene
660 cyclone variability in the Central Pacific using sedimentary records from Tahaa, French
661 Polynesia. Quaternary Science Reviews 77, 181-189, 2013.

662 Vött, A., Handl, M. and Brückner, H. Rekonstruktion holozäner Umweltbedingungen in
663 Akarnanien (Nordwestgriechenland) mittels Diskriminanzanalyse von geochemischen
664 Daten. Geologica et Palaeontologica 36: 123-147, 2002.

665 Wilhelm, B., Arnaud, F., Sabatier, P., Crouzet, Ch., Elodie, B., Eric, Ch., Jean-Robert, D.,
666 Frederic, G., Emmanuel, M., Jean-Louis, R., Kazuyo, T., Edouard, B., and Jean-Jacques,
667 D.: 1400 years of extreme precipitation patterns over the Mediterranean French Alps and
668 possible forcing mechanisms, Quaternary Research; 78, 1-12, 2012.

669 Wolfe, B.B., Hall, R.I., Last, W.M., Edwards, T.W.D., English, M.C., Karst-Riddoch, T.L.,
670 Paterson, A., and Palmi, R.: Reconstruction of multi-century flood histories from

671 oxbow lake sediments, Peace-Athabasca Delta, Canada. *Hydrol. Process*, 20, 4131- 4153,
672 2006.

673 Woodruff, J.D., Donnelly, J.P., Okusu, A.: Exploring typhoon variability over the mid-to-late
674 Holocene: evidence of extreme coastal flooding from Kamikoshiki, Japan. *Quaternary*
675 *Science Reviews* 28, 1774-1785, 2009.

676 Zielhofer, C., Faust, D., Baena, R., Diaz del Olmo, F., Kadereit, A., Moldenhauer, K.-M.,
677 Porras, A.: Centennial-scale late Pleistocene to mid-Holocene synthetic profile of the
678 Medjerda floodplain (Northern Tunisia). *The Holocene* 14, 851–861, 2004.

679 Zielhofer, C and Faust, D.: Mid- and Late Holocene fluvial chronology of Tunisia, *Quaternary*
680 *Science Reviews* ,Volume 27, Issues 5-6, , Pages 580-588, March 2008.

681 Zhu, Y. and Weindorf, D.: Determination of soil calcium using field portable X-ray fluores-
682 cence. *Soil Science*, 174 (3), 151-155, 2009.

683

684

685

686

687

688

689

690

691

692

693

694

695

696 **Figures Captions**

697 **Figure 1.** Location of the study area of El Bibane Lagoon (EBL) South East of Tunisia (A)
698 and the geological map of South Eastern Tunisia (Modified from the Geological map of
699 Tunisia 1/500000 after Ben Haj Ali et al., 1985) (B).

700 **Figure 2.** Variation of the annual precipitations of the Medenine and Tataouine meteorological
701 stations during the period between 1900 and 2000 (DGRE, 2010). Dashed line: mean annual
702 precipitation.

703 **Figure 3.** Location of the investigated surface samples from the catchment basin and from the
704 El Bibane Lagoon.

705 **Figure 4.** Microtextural photos under binocular observation of five representative samples
706 from the catchment basin of El Bibane Lagoon. S3 Marine sample; S8 and S11: Fessi River
707 samples; S17 and S18: Dunes samples (Diameter of the photos: 3 cm; G x 6.5).

708 **Figure 5.** Particle size distributions (<2000 μ m) of representative samples from the catchment
709 basin and the El Bibane Lagoon.

710 **Figure 6:** Distribution of the mean size of the samples collected in the Fessi River

711 **Figure 7.** Distribution map of major and trace elements in surface sediments from catchment
712 basin and the El Bibane lagoon.

713 **Figure 8.** Principal Component Analysis (PCA) loadings plot of major and trace elements
714 concentrations displaying the three main sources: marine, fluvial and aeolian sand dune.

715 **Figure 9.** Distribution of the investigated surface samples from the watershed and the El
716 Bibane Lagoon on a cross-plot Fe/Ca *versus* Ti/Ca

717 **Figure 10.** $^{210}\text{Pb}_{\text{ex}}$ and ^{137}Cs activity-depth profiles along the core BL12-10. SR:
718 sedimentation rate (cm yr $^{-1}$).

719 **Figure 11.** Records of eight geochemical elements (expressed in percentage or ppm) *versus*
720 depth in core BL12-10.

721 **Figure 12.** (a) Paleoflood records in sedimentary archive of core BL12-10 based on elemental
722 ratios of Fe/Ca and Ti/Ca and grain size analysis (clay + silt ; fraction <63µm). Triangles
723 indicate the age control obtained using ^{210}Pb and ^{137}Cs along the core. Colored areas display
724 the three periods of floods recorded in the core (FL1, FL2 and FL3). (b) Observed rainfall
725 record since, 1932 in Medenine and Tataouine stations, is also shown.

726 **Tables captions**

727 **Table 1.** Geographic location and GPS coordinate of the studied samples

728 **Table 2.** Grain size statistical analysis of surface samples from the watershed of the El Bibane
729 Lagoon.

730 **Table 3.** XRF analysis results of the major and trace element in studied samples.

731 **Table 4.** Activities of radionuclides ^{210}Pb , ^{137}Cs and ^{226}Ra along the core BL12-10.

732 **Table 5.** Grain size statistical analysis along the core BL12-10.

733

734

735

736

737

738

739

740

741

742

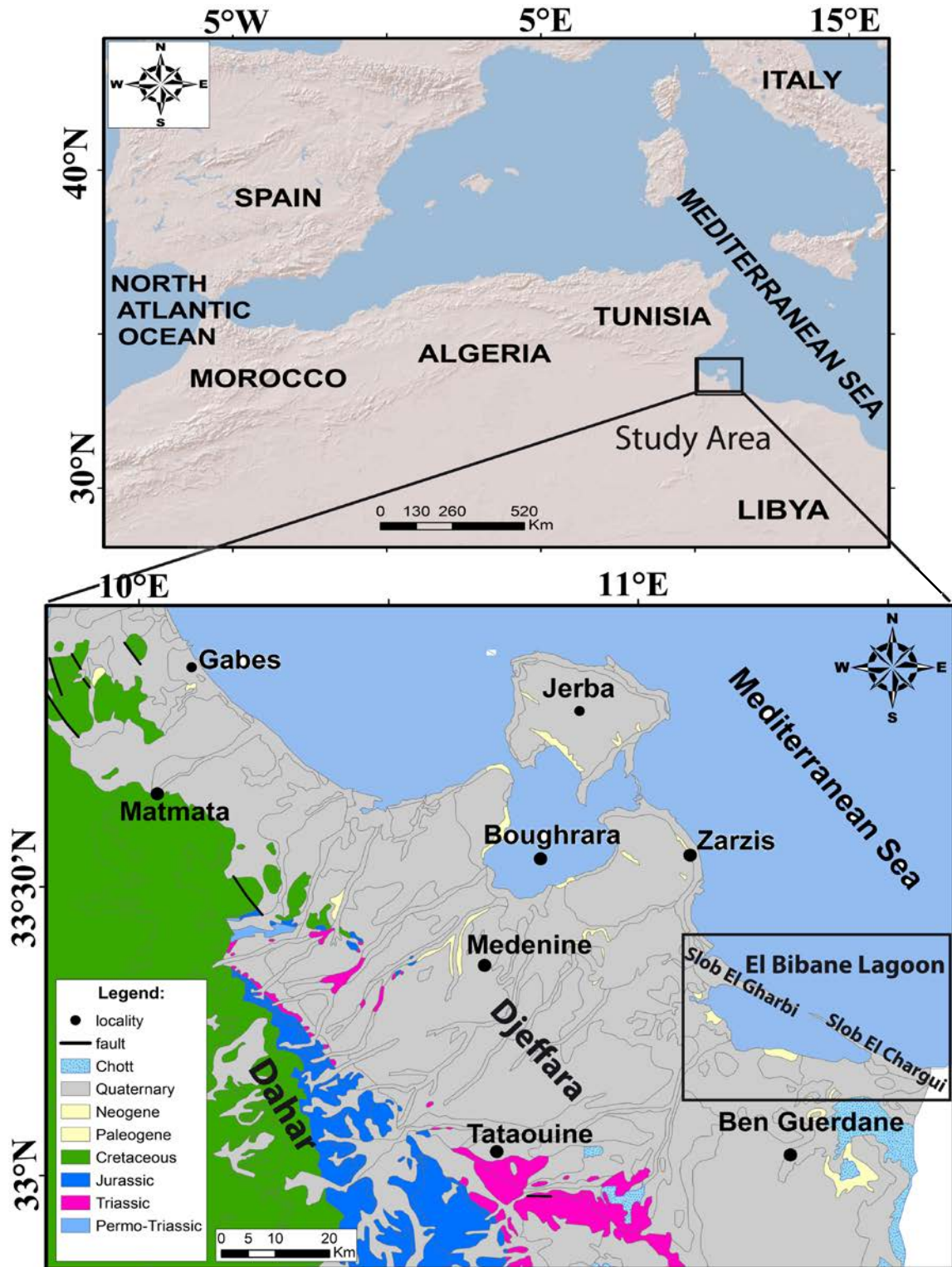
743

744

745

746 **Figure 1**

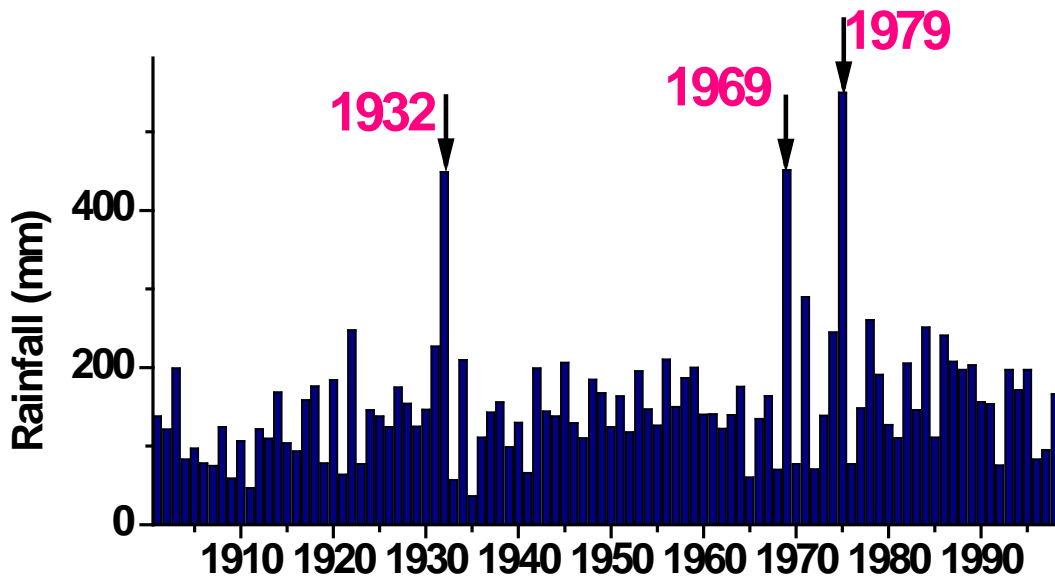
747



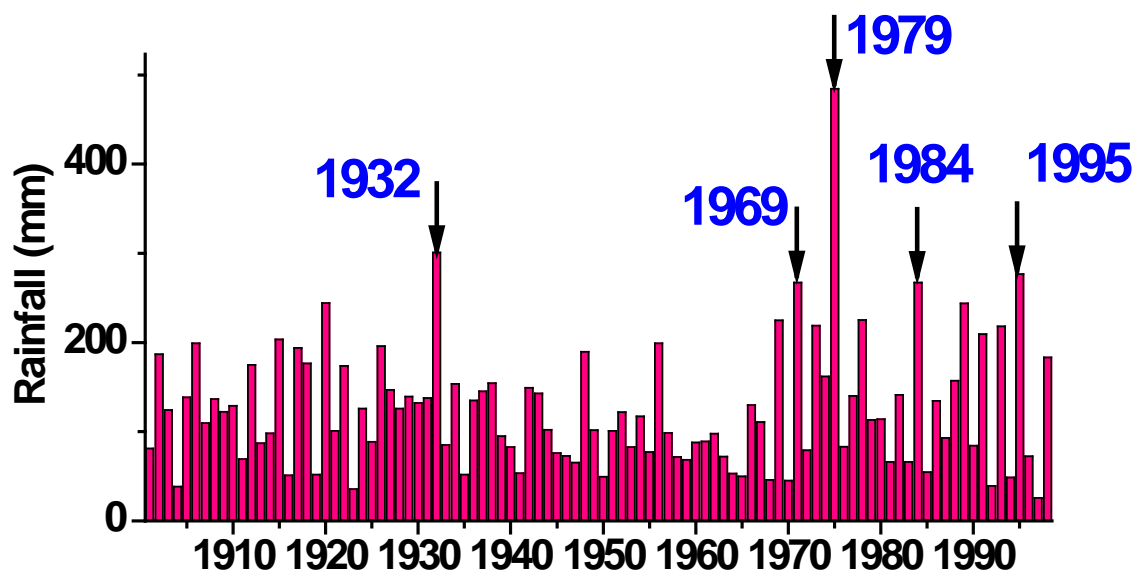
748

749

750



Annual Rainfall of the Medenine watershed



Annual rainfall of the Tataouine watershed

752

753

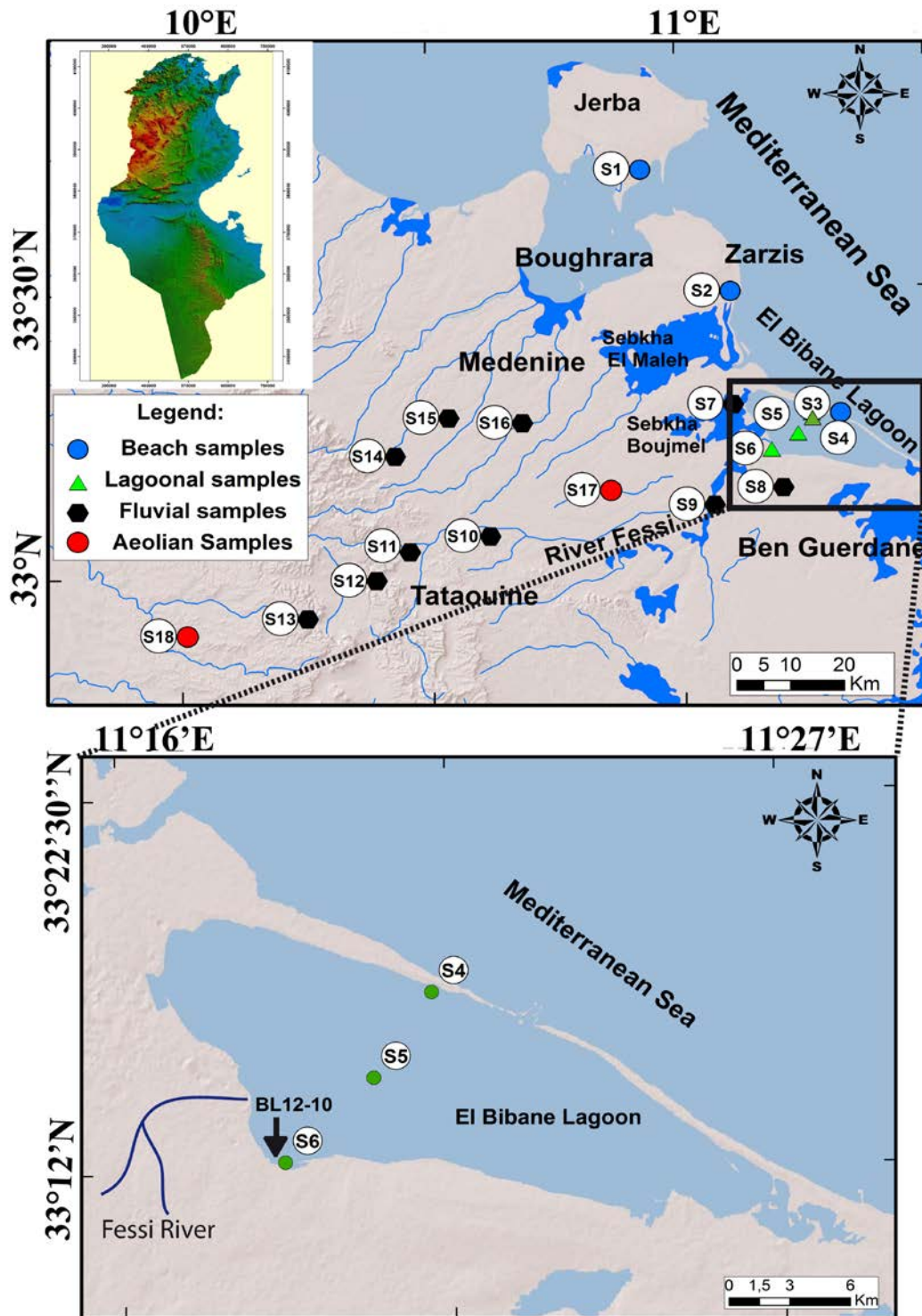
754

755

756

757 **Figure 3**

758



759

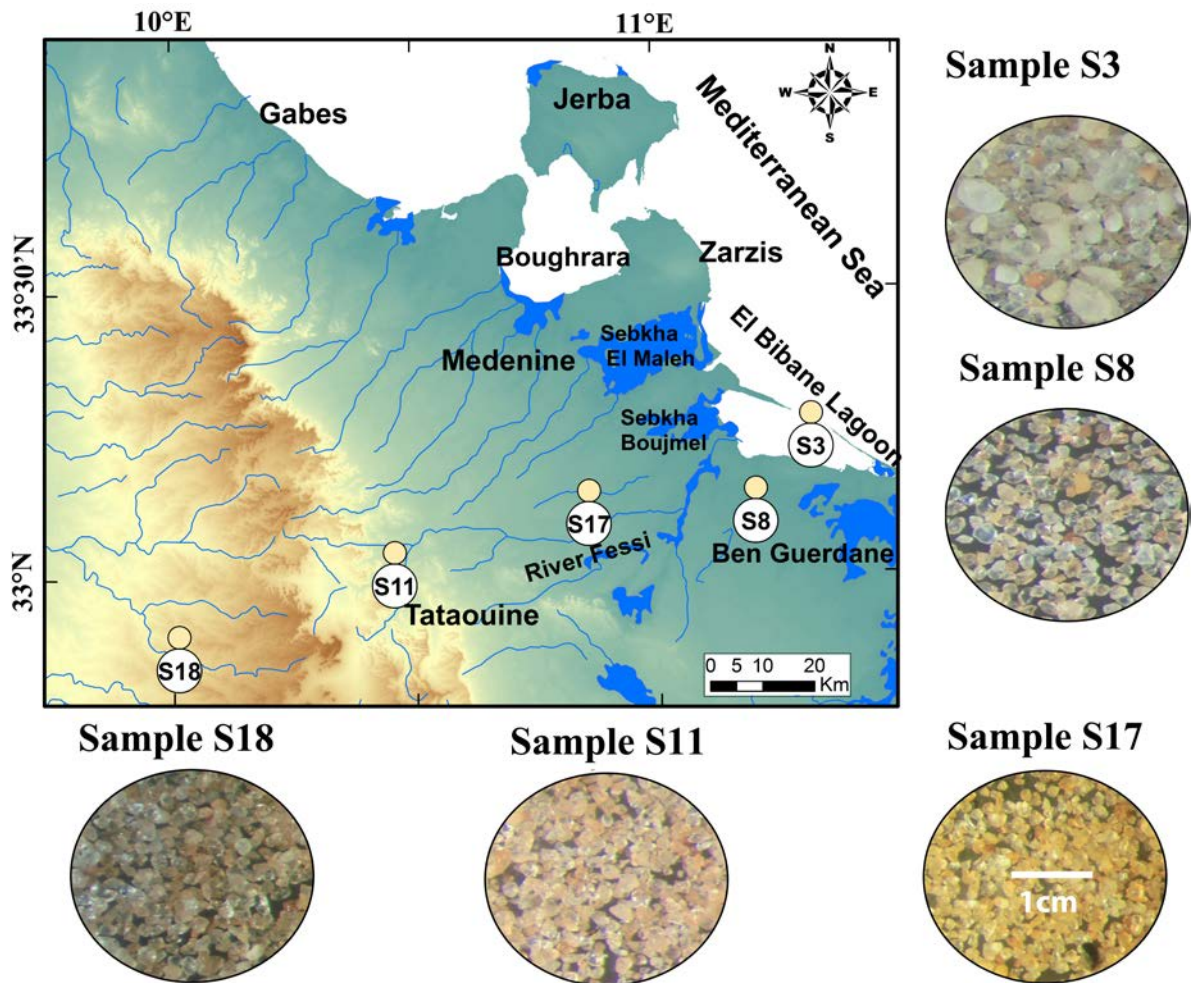
760

761

762

763 **Figure 4**

764



765

766

767

768

769

770

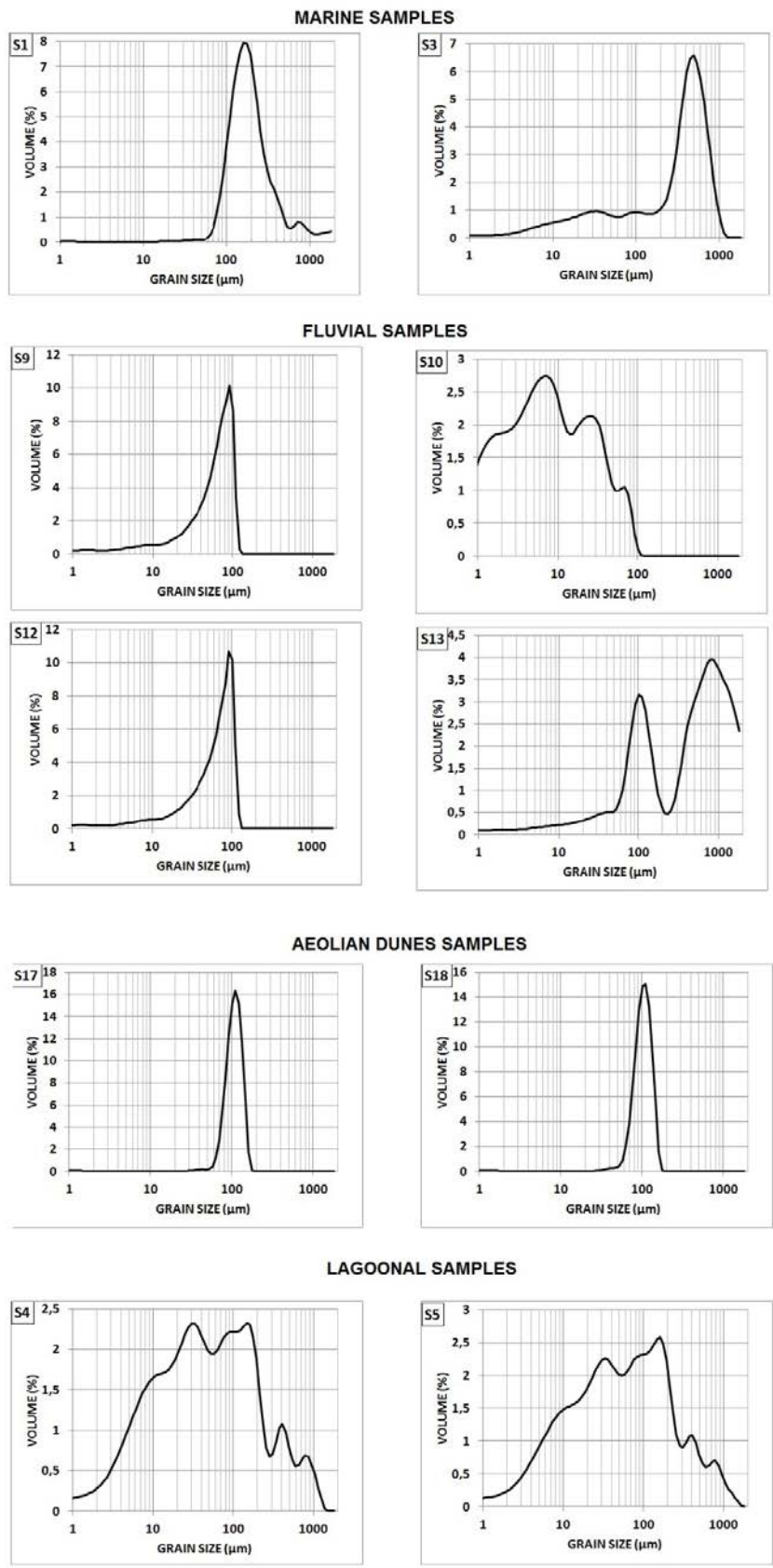
771

772

773

774

775



778 **Figure 6**

779

780

781

782

783

784

785

786

787

788

789

790

791

792

793

794

795

796

797

798

799

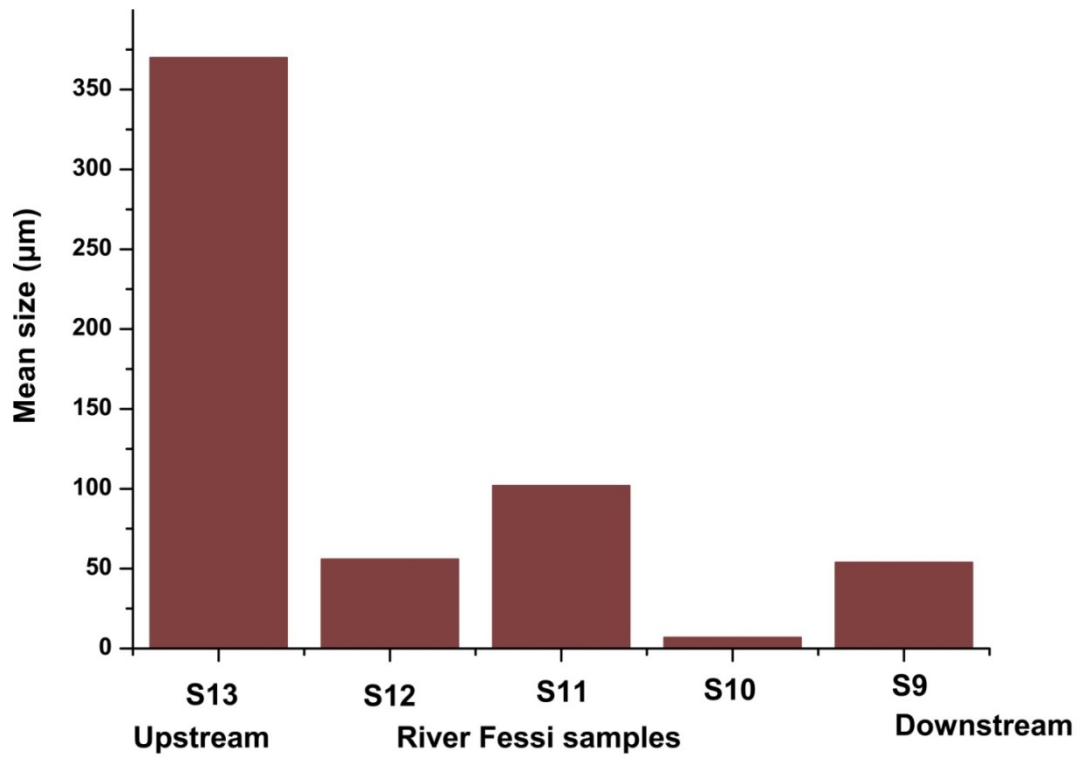
800

801

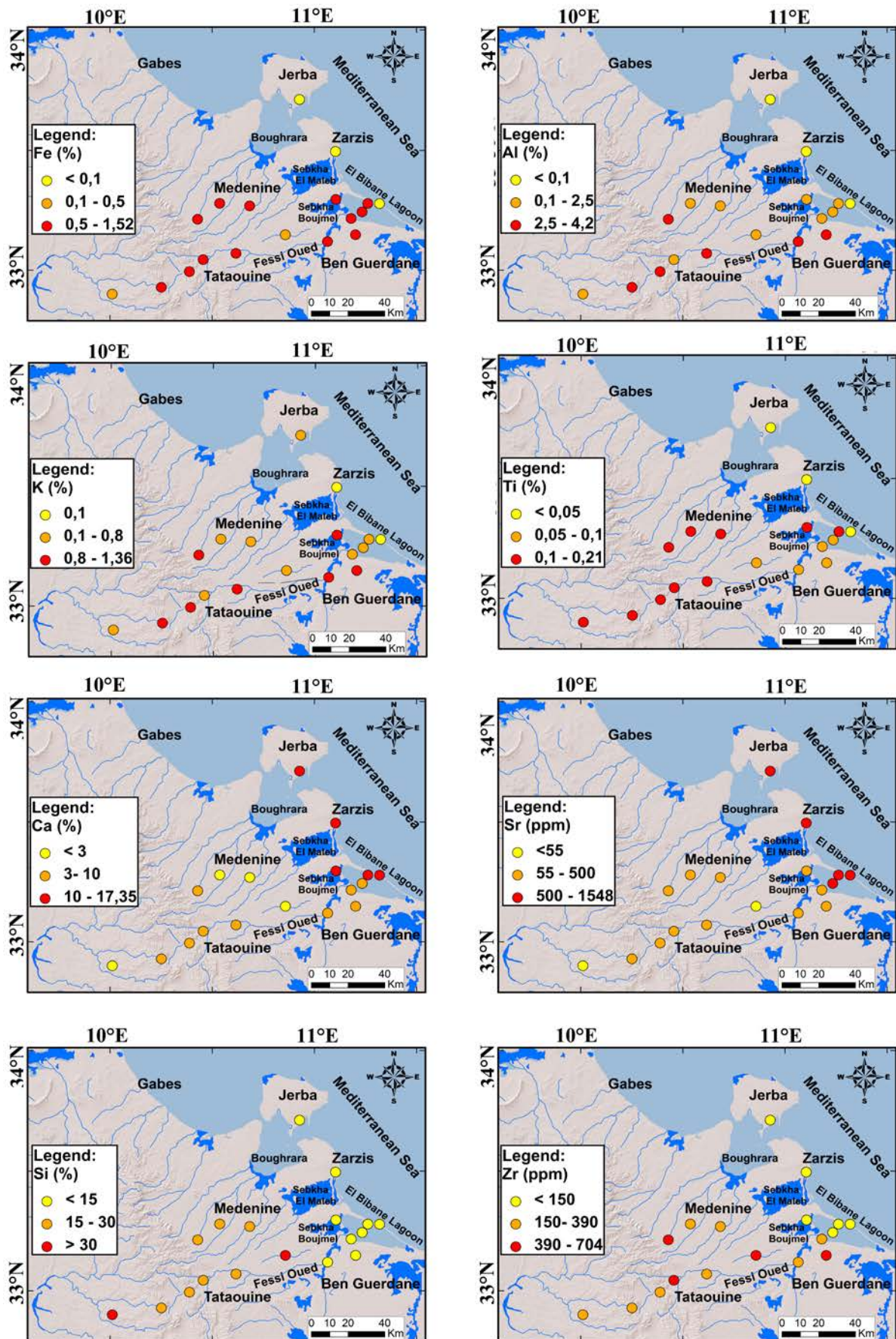
802

803

804

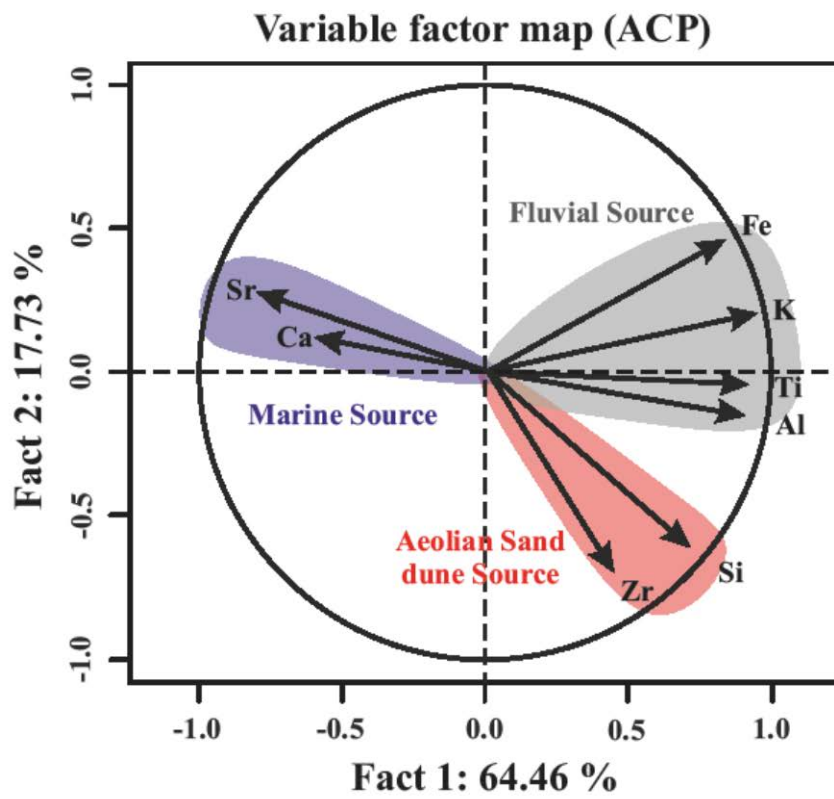


805 **Figure 7**



807 **Figure 8**

808



809

810

811

812

813

814

815

816

817

818

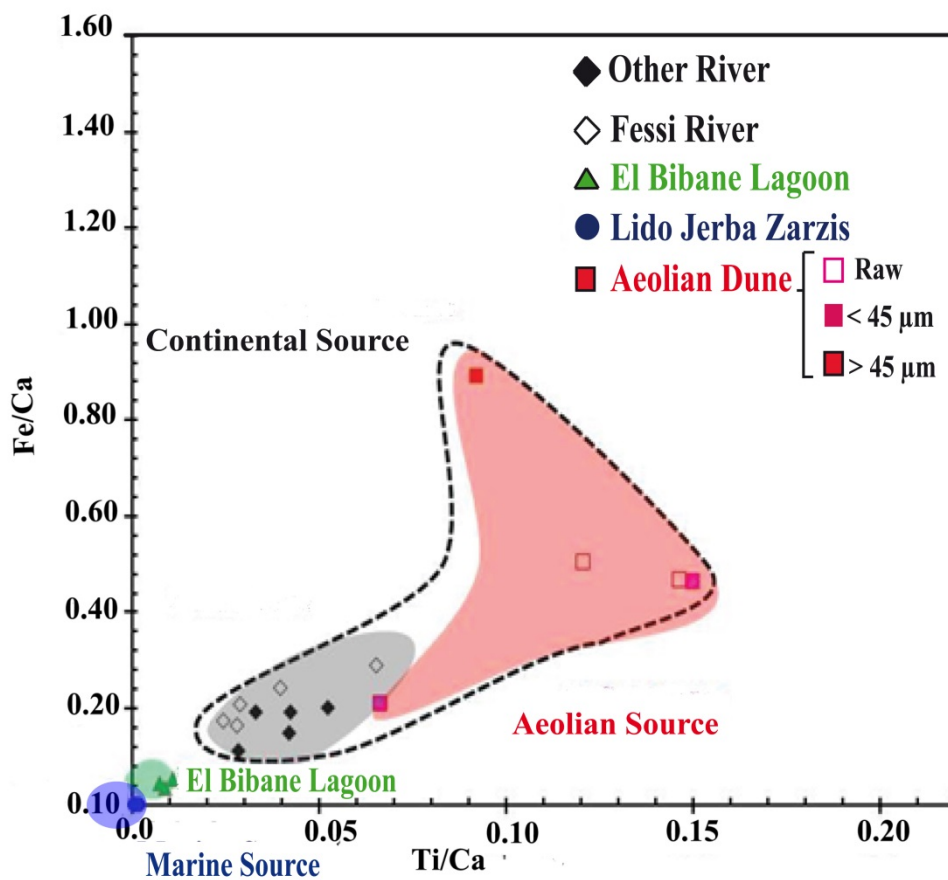
819

820

821

822 **Figure 9**

823



824

825

826

827

828

829

830

831

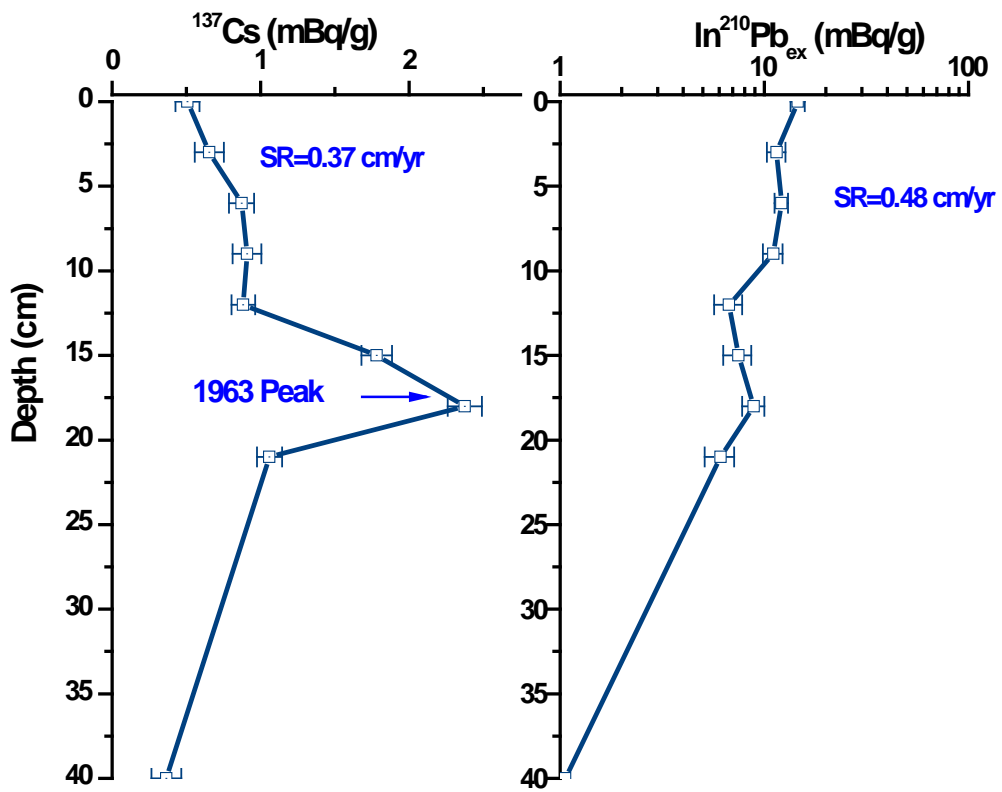
832

833

834

835

836 **Figure 10**



837

838

839

840

841

842

843

844

845

846

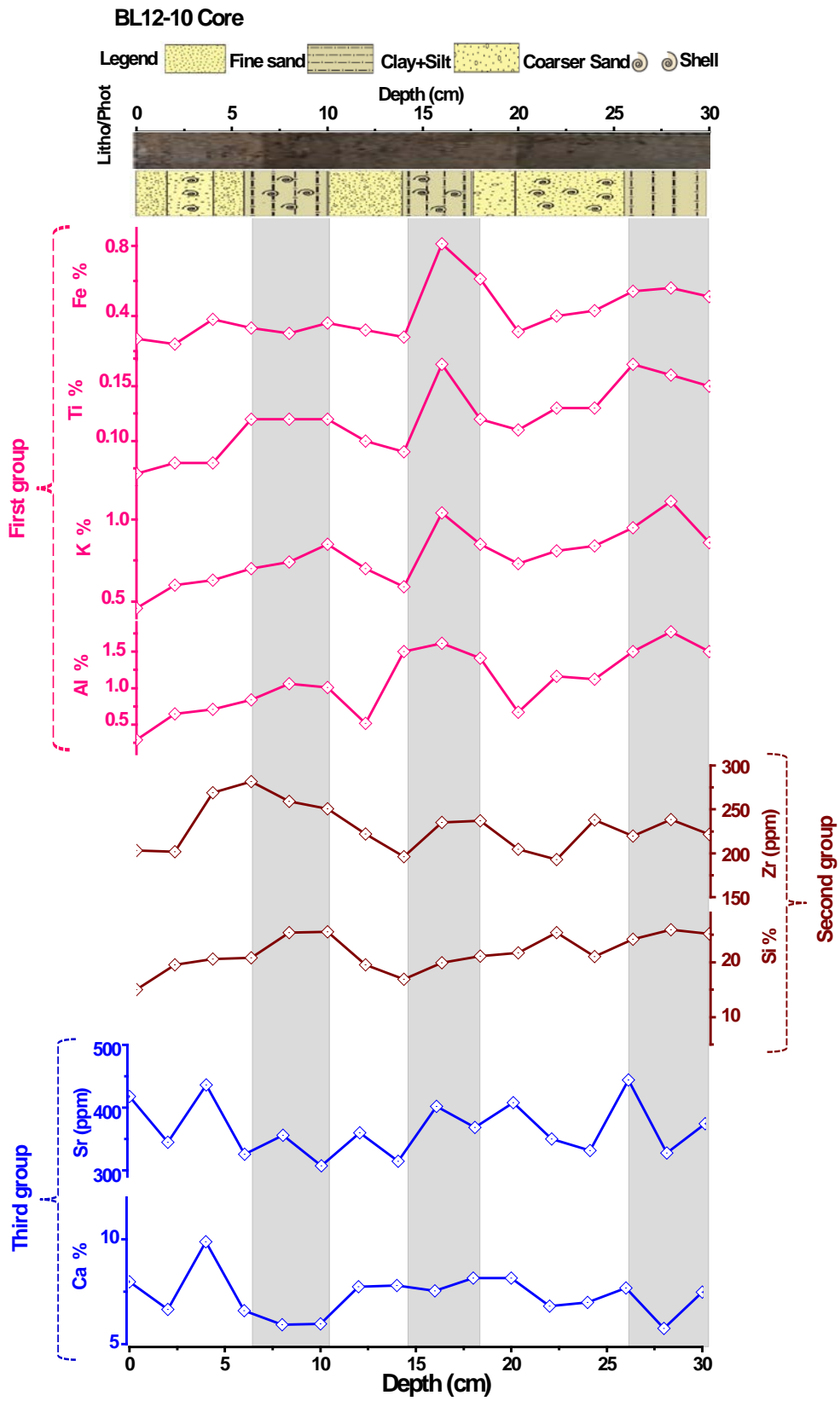
847

848

849

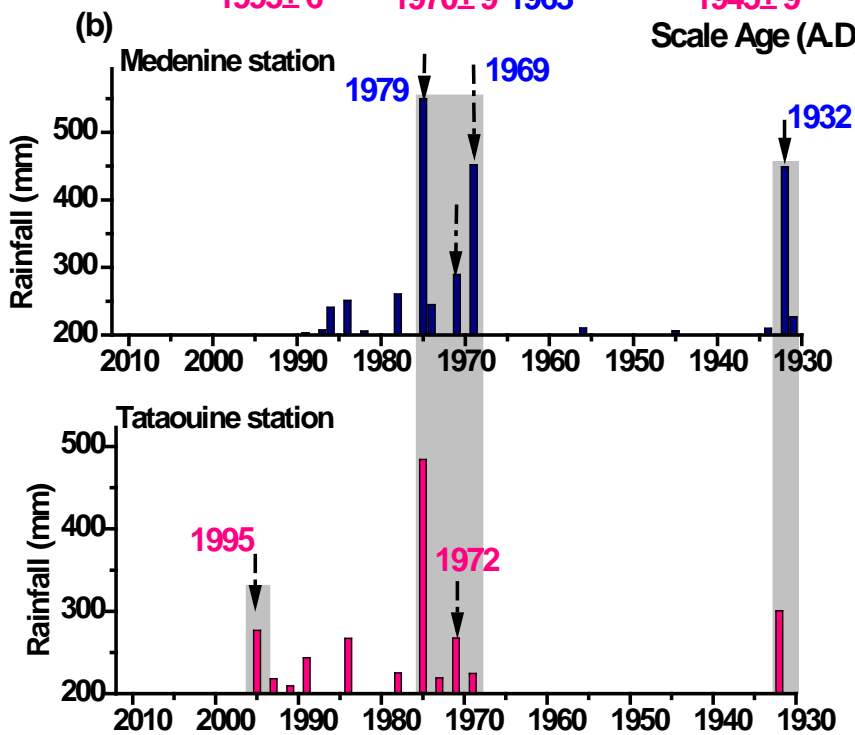
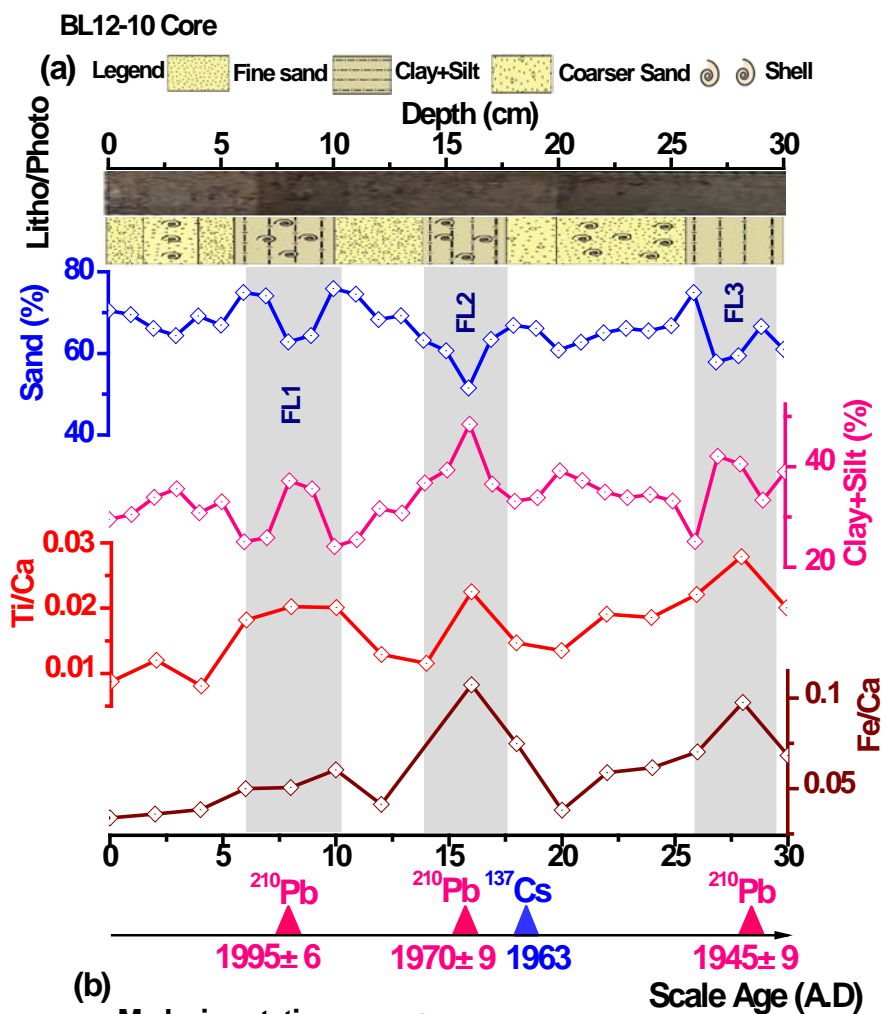
850

851 **Figure 11**



852

853



Last century historical rainfall of the Tataouine and Medenine stations

856 **Table 1**

Sample	Locality	GPS coordinates	
		Latitude	Longitude
S1	Beach	33°45'12.4"	10°59'57.9"
S2	Beach	33°35'31.5"	11°04'45.2"
S3	Beach	33°16'39.9"	11°17'39.6"
S4	Lagoon	33°15'38.7"	11°16'40.6"
S5	Lagoon	33°14'0.01"	11°17'.02"
S6	Lagoon	33°13'52.3"	11°06'31.3"
S7	River	33°16'52.3"	11°07'31.3"
S8	River	33°08'03.0"	11°06'51.6"
S9	River	33°03'32.1"	11°02'00.4"
S10	River	33°04'13.6"	10°40'56.0"
S11	River	32°59'23.4"	10°28'12.7"
S12	River	32°55'18,0"	10°24'15.1"
S13	River	32°55'09.7"	10°22'35,3"
S14	River	33°03'38.0"	10°24'05.6"
S15	River	33°09'59.2"	10°21'35.8"
S16	River	33°12'25.37"	10°26'46.78"
S17	Aeolian	33°07'18.9"	10°44'58.6"
S18	Aeolian	32°50'28.4"	10°13'43.7"

857

858

859

860

861

862

863

864

865 **Table 2**

Sample name	Sampling Locality	SAMPLE TYPE	TEXTURAL GROUP	SEDIMENT NAME
S1	Beach	Unimodal, Moderately Sorted	Sand	Moderately Sorted Fine Sand
S2		Unimodal, Moderately Sorted	Sand	Moderately Sorted Fine Sand
S3		Unimodal, Very Poorly Sorted	Muddy Sand	Very Coarse Silty Coarse Sand
S4	Surface sediments El Bibane Lagoon	Polymodal, Very Poorly Sorted	Sandy Mud	Very Fine Sandy Very Coarse Silt
S5		Unimodal, Moderately Sorted	Muddy Sand	Very Coarse Silty Fine Sand
S6		Bimodal, Poorly Sorted	Muddy Sand	Very Coarse Silty Very Fine Sand
S9	Fessi River	Unimodal, Poorly Sorted	Muddy Sand	Very Coarse Silty Very Fine Sand
S10		Trimodal, Poorly Sorted	Mud	Fine Silt
S11		Unimodal, Well Sorted	Sand	Well Sorted Very Fine Sand
S12		Unimodal, Poorly Sorted	Muddy Sand	Very Coarse Silty Very Fine Sand
S13		Bimodal, Poorly Sorted	Muddy Sand	Very Coarse Silty Coarse Sand
S17	Sand dune	Unimodal, Very Well Sorted	Sand	Very Well Sorted Very Fine Sand
S18		Unimodal, Well Sorted	Sand	Well Sorted Very Fine Sand

866

867 **Table 2. Continued**

868

Sample name	FOLK AND WARD METHOD (μm)				MODE 1 (μm)	MODE 2 (μm)	MODE 3 (μm)
	MEAN	SORTING	SKEWNESS	KURTOSIS			
S1	196.20	1.79	0.23	1.31	169.10		
S2	249.10	1.81	0.18	1.11	203.70		
S3	204.20	4.23	-0.66	1.02	517.80		
S4	43.46	4.68	-0.03	0.93	154.00	31.54	96.60
S5	112.50	1.81	-0.22	1.20	116.40		
S6	80.39	3.15	-0.24	1.70	106.00	429.70	
S9	54.69	2.24	-0.57	1.49	96.60		
S10	7.13	3.89	0.00	0.84	7.09	26.17	73.02
S11	102.50	1.34	-0.24	1.22	116.40		
S12	56.17	2.25	-0.57	1.42	96.60		
S13	370.90	3.90	-0.41	0.88	825.40	106.00	
S17	110.50	1.26	-0.13	1.01	116.40		
S18	106.40	1.29	-0.13	1.03	116.40		

869

870

871

872

873

874 **Table 3**

Sample name	Locality	Zr (ppm)	Sr (ppm)	Ca (%)	Fe (%)	Ti (%)	K (%)	Al (%)	Si (%)
S1	Beach	113	1497	14.67	0.00	0.03	0.14	0.00	9.71
S2	Beach	41	1548	14.51	0.00	0.01	0.10	0.00	6.85
S3	Beach	24	899	13.36	0.00	0.01	0.10	0.00	8.38
S4	Lagoon	133	1035	17.35	0.75	0.13	0.74	0.40	15.00
S5	Lagoon	85	747	9.00	0.47	0.10	0.47	0.18	8.70
S6	Lagoon	203	418	7.90	0.27	0.07	0.56	0.69	12.00
S7	River	134	358	17.35	0.75	0.13	1.10	2.08	15.00
S8	River	488	90	9.00	0.53	0.10	0.81	2.60	8.70
S9	River	178	97	7.90	0.98	0.07	1.13	2.76	12.00
S10	River	235	105	7.30	1.52	0.21	1.36	4.20	26.16
S11	River	704	92	6.00	0.59	0.16	0.56	2.20	26.93
S12	River	275	173	7.37	1.22	0.21	1.12	3.60	27.43
S13	River	391	123	7.35	1.28	0.18	0.93	2.60	27.13
S14	River	458	186	7.16	0.79	0.20	0.87	2.70	26.18
S15	River	350	102	3.95	0.59	0.17	0.77	2.40	29.08
S16	River	263	73	3.22	0.62	0.11	0.74	1.80	25.62
S17	Aeolian	473	52	0.80	0.40	0.10	0.75	2.50	33.38
S18	Aeolian	357	54	0.81	0.38	0.12	0.74	2.40	33.09

875

876

877

878

879

880

881

882

883

884

885

886

887

888

889 **Table 4**

Sample name	Locality	Zr (ppm)	Sr (ppm)	Ca (%)	Fe (%)	Ti (%)	K (%)	Al (%)	Si (%)
S1	Beach	113	1497	14.67	0.00	0.03	0.14	0.00	9.71
S2	Beach	41	1548	14.51	0.00	0.01	0.10	0.00	6.85
S3	Beach	24	899	13.36	0.00	0.01	0.10	0.00	8.38
S4	Lagoon	133	1035	17.35	0.75	0.13	0.74	0.40	15.00
S5	Lagoon	85	747	9.00	0.47	0.10	0.47	0.18	8.70
S6	Lagoon	203	418	7.90	0.27	0.07	0.56	0.69	12.00
S7	River	134	358	17.35	0.75	0.13	1.10	2.08	15.00
S8	River	488	90	9.00	0.53	0.10	0.81	2.60	8.70
S9	River	178	97	7.90	0.98	0.07	1.13	2.76	12.00
S10	River	235	105	7.30	1.52	0.21	1.36	4.20	26.16
S11	River	704	92	6.00	0.59	0.16	0.56	2.20	26.93
S12	River	275	173	7.37	1.22	0.21	1.12	3.60	27.43
S13	River	391	123	7.35	1.28	0.18	0.93	2.60	27.13
S14	River	458	186	7.16	0.79	0.20	0.87	2.70	26.18
S15	River	350	102	3.95	0.59	0.17	0.77	2.40	29.08
S16	River	263	73	3.22	0.62	0.11	0.74	1.80	25.62
S17	Aeolian	473	52	0.80	0.40	0.10	0.75	2.50	33.38
S18	Aeolian	357	54	0.81	0.38	0.12	0.74	2.40	33.09

890

891

892

893

894

895

896

897

898

899

900

901

902

903

904 **Table 5**

DEPTH (cm)	Sample name	SAMPLE TYPE	TEXTURAL GROUP	SEDIMENT NAME
1	BL12-10-1	Bimodal, Poorly Sorted	Muddy Sand	Very Coarse Silty Very Fine Sand
2	BL12-10-2	Trimodal, Very Poorly Sorted	Muddy Sand	Very Coarse Silty Very Fine Sand
3	BL12-10-3	Trimodal, Poorly Sorted	Muddy Sand	Very Coarse Silty Very Fine Sand
4	BL12-10-4	Trimodal, Very Poorly Sorted	Muddy Sand	Very Coarse Silty Very Fine Sand
5	BL12-10-5	Trimodal, Poorly Sorted	Muddy Sand	Very Coarse Silty Very Fine Sand
6	BL12-10-6	Trimodal, Poorly Sorted	Muddy Sand	Very Coarse Silty Very Fine Sand
7	BL12-10-7	Trimodal, Poorly Sorted	Muddy Sand	Very Coarse Silty Very Fine Sand
8	BL12-10-8	Bimodal, Poorly Sorted	Muddy Sand	Very Coarse Silty Very Fine Sand
9	BL12-10-9	Bimodal, Poorly Sorted	Muddy Sand	Very Coarse Silty Very Fine Sand
10	BL12-10-10	Trimodal, Poorly Sorted	Muddy Sand	Very Coarse Silty Very Fine Sand
11	BL12-10-11	Trimodal, Poorly Sorted	Muddy Sand	Very Coarse Silty Very Fine Sand
12	BL12-10-12	Trimodal, Very Poorly Sorted	Muddy Sand	Very Coarse Silty Very Fine Sand
13	BL12-10-13	Trimodal, Poorly Sorted	Muddy Sand	Very Coarse Silty Very Fine Sand
14	BL12-10-14	Trimodal, Very Poorly Sorted	Muddy Sand	Very Coarse Silty Very Fine Sand
15	BL12-10-15	Trimodal, Poorly Sorted	Muddy Sand	Very Coarse Silty Very Fine Sand
16	BL12-10-16	Trimodal, Very Poorly Sorted	Muddy Sand	Very Coarse Silty Very Fine Sand
17	BL12-10-17	Trimodal, Very Poorly Sorted	Muddy Sand	Very Coarse Silty Very Fine Sand
18	BL12-10-18	Trimodal, Very Poorly Sorted	Muddy Sand	Very Coarse Silty Very Fine Sand
19	BL12-10-19	Trimodal, Very Poorly Sorted	Muddy Sand	Very Coarse Silty Very Fine Sand
20	BL12-10-20	Bimodal, Poorly Sorted	Muddy Sand	Very Coarse Silty Very Fine Sand
21	BL12-10-21	Bimodal, Poorly Sorted	Muddy Sand	Very Coarse Silty Very Fine Sand
22	BL12-10-22	Trimodal, Poorly Sorted	Muddy Sand	Very Coarse Silty Very Fine Sand
23	BL12-10-23	Trimodal, Poorly Sorted	Muddy Sand	Very Coarse Silty Very Fine Sand
24	BL12-10-24	Bimodal, Poorly Sorted	Muddy Sand	Very Coarse Silty Very Fine Sand
25	BL12-10-25	Trimodal, Poorly Sorted	Muddy Sand	Very Coarse Silty Very Fine Sand
26	BL12-10-26	Trimodal, Poorly Sorted	Muddy Sand	Very Coarse Silty Very Fine Sand
27	BL12-10-27	Trimodal, Very Poorly Sorted	Muddy Sand	Very Coarse Silty Very Fine Sand
28	BL12-10-28	Trimodal, Very Poorly Sorted	Muddy Sand	Very Coarse Silty Very Fine Sand
29	BL12-10-29	Trimodal, Poorly Sorted	Muddy Sand	Very Coarse Silty Very Fine Sand
30	BL12-10-30	Bimodal, Poorly Sorted	Muddy Sand	Very Coarse Silty Very Fine Sand

905

906

907

908

909